Centre for Geo-Information

Thesis Report GIRS-2003-013

Fusion of CASI and LiDAR data for classification of vegetation in floodplains in The Netherlands

Mauricio Labrador García

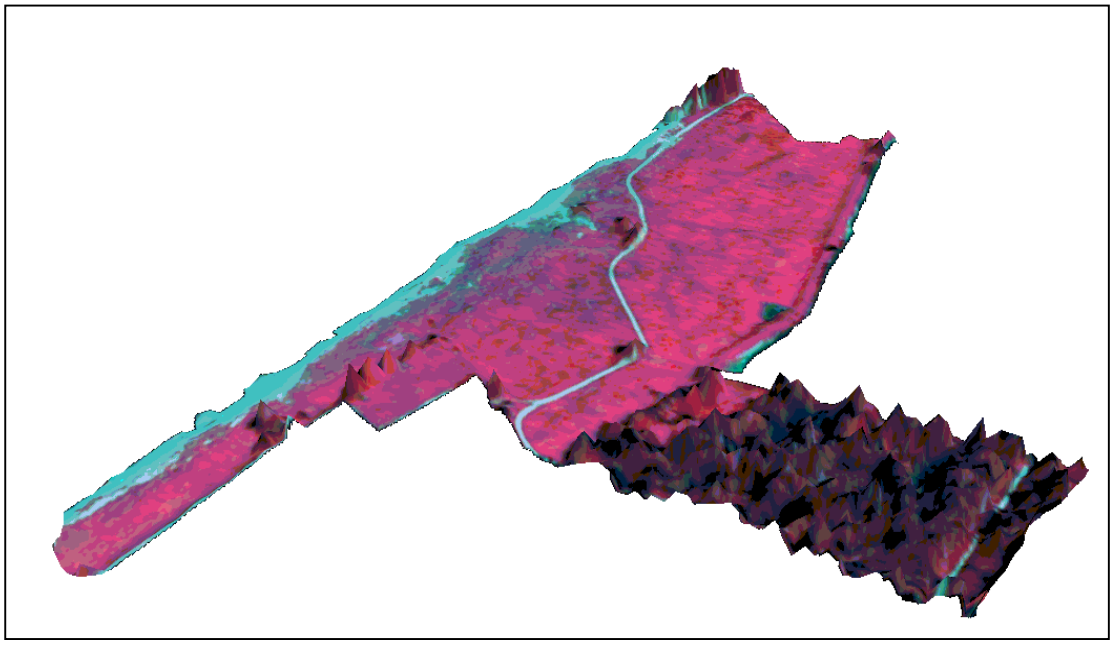

March 2003

WAGENINGEN UNIVERSITY

WAGENINGEN UR

I. Acknowledgements

I would like to express my gratitude to many people who has participated in different ways in the development of this research.

First to my supervisors Drs. Gertjan Geerling[1] and Dr. Ir. Jan Clevers for their guidance and support. Without their help and good advise it would have been impossible to complete this study. Especially to Gertjan for his continuous trips Nijmegen-Wageningen, which made possible a better contact and exchange of ideas and to Jan Clevers for his 'full-time availability' and very good and useful comments about my work.

Also I would like to express my gratitude to Dr. Monica Wachowicz, who contributed with important suggestions during the first steps of this research in a very kind way.

I cannot forget Dr. Gerrit Epema, who encouraged me to start this master and understood my situation when I encountered some difficulties the first time I tried to come to The Netherlands.

Also I am very glad for the time I worked in the 'MSc room'. The environment created among all the students was excellent and the discussions about our work very productive. Especially the help and support from Giuseppe (important his 'feeding support' at *the trattoria*, during the last stressed weeks, considering that supermarkets are not open anymore after 10 PM). Also I would like to express my sincere gratitude to Achilleas, the other member of the *pistola* team, who helped me and with whom the exchange of ideas was continuous and very useful for our work.

Some people did not participate directly in this study but helped me and were very important for me during my stay in Wageningen. They deserve to have special mention in this last part of the acknowledgements and to them this work is dedicated. They are my parents Amado y Carmita and my brothers and sisters Sergio, Sofia and Gustavo who supported me from the *warm* distance all the time. Also to my girlfriend Sonia *(TQ)*, who ended up knowing about remote sensing more than she expected before coming to Wageningen.

[1] Special chair for nature management of stream corridors. Dept. of environmental Studies. University of Nijmegen.

II. Abstract

In recent years remote sensing has become a very important tool to study and monitor many processes. Among them, the analysis of natural vegetation is one of the most important ones and it is a field under continuous research. In this study, the classification of natural vegetation according to different structural classes is needed as a factor to calculate the hydraulic roughness of floodplains. The hydraulic roughness is one of the parameters that help calculate the water discharge capacity of the river and so it is a crucial parameter for river management.

The use of altimetry laser scanning data (LiDAR) and hyperspectral imagery (CASI) is investigated to classify natural vegetation in a floodplain of the river Waal, known as the Millingerwaard, in The Netherlands. The structural information given by the LiDAR image was expected to improve the classification results, adding extra structural information to the classical 'spectral analysis approach'.

A methodology to fuse and classify the CASI and LiDAR images was developed. The LiDAR image was analyzed and transformed in such a way that structural information could be extracted in the form of grid maps and fused with the CASI image. The Maximum Likelihood classifier was used to classify the single and fused images. Error matrices were derived to compare and to analyze differences. Decision Tree analysis was also tried as an alternative method to classify the fused image.

The fusion of CASI and LiDAR images improved the overall accuracy of the classification (from 55.60% to 63.52%) compared to the classification using spectral information only. Also important conclusions concerning the information added by the LiDAR image were drawn from the results. At the end a list of recommendations that can be useful for further research in this field is given.

This study was intended to give the first steps into the promising idea of integrating hyperspectral and laser altimetry information. Further research should be done in this direction to explore the enormous possibilities that these two data sets can offer for remote sensing analysis.

Keywords: Laser altimetry, LiDAR, hyperspectral, CASI, image fusion, floodplains, natural vegetation, structural classes, Maximum Likelihood, Decision Tree analysis.

III. List of figures

IV. List of tables

V. List of acronyms

ALS	Airborne Laser Altimetry
AOI	Area Of Interest
CART	Classification And Regression Trees
CASI	Compact Airborne Spectrographic Imager
DGPS	Differential Global Positioning System
DEM	Digital Elevation Model
DTM	Digital Terrain Model
IMU	Inertial Measurement Unit
LADAR	Laser Detection and Ranging
LiDAR	Light Detection and Ranging
LVIS	Laser Vegetation Imaging Sensor
MAX	Maximum
MIN	Minimum
MLC	Maximum Likelihood Classifier
PCA	Principal Component Analysis
POS	Position Orientation System
SHOALS	Scanning Hydrographic Operational Airborne LiDAR Survey
SLICER	Scanning LiDAR Imager of Canopies by Echo Recovery
STD	Standard Deviation

Table of contents

1 Introduction

1.1 Background

Napoleon described The Netherlands as "nothing more than a silty delta formed from the great rivers of the empire". This idea is not far from reality if we consider that the land consists to a large extent of sediments deposited by the Meuse and the Rhine over de millennia (RIZA, 1999).

This means that people living near the Netherlands' great rivers have always had to be alert to danger. Down through the centuries people have built and made dikes higher to protect from floods. Nevertheless the idea of raising the dikes further is no longer seen as appropriate.

The dikes were a solution, but they led to the narrowing of the river floodplains and to the accumulation of sediments on the riverbed through the years. Thus, increasing continuously the height of the dikes is a 'vicious circle' that leads to higher ground levels of the floodplains and larger inundation depths, as well as more damage when a dike should burst.

The new water management policy is creating more space for the rivers, making a more flexible system that can cope with floods. At the same time, those spaces offer unique opportunities for nature development and this is also one of the important points of the new policies.

However, nature development must not compromise flood protection. For example, large areas of floodplain forest increase flow resistance, raising the risk of flood in the land behind the dikes.

A compromise between flood protection and nature development is the central pillar of the new water management policy for the important rivers in the Netherlands.

To achieve this, the river management requires a constant updating of the vegetation mapping in the floodplains since vegetation plays a very important role in discharge capacity of the river. So many efforts are being done to find a way to monitor vegetation changes at different scales in a fast and accurate way. Remote sensing techniques may provide the appropriate tools for this.

The use of multispectral imagery (CASI) and Laser Altimetry (LiDAR) is expected to be of good use to classify vegetation in the floodplains and is being investigated for this purpose.

The study area where the study is carried out is a part of a floodplain known as the Millingerwaard, near the river Rhine, of approximately 1 km^2. The central coordinates of the study area are 196.75, 431.5 (Dutch coordinate system). If the results obtained are satisfactory, the method could be extended to larger areas.

Fig. 1: Study area

1.2 Problem definition

Traditional classification of vegetation based only on spectral information has shown some limits. Conventional passive sensors produce only two-dimensional (*x* and *y*) images, which cannot fully represent the complex 3-dimensional structure of, for instance, vegetation (Lefsky *et al.*, 2002)

The classification we perform in this study is based on the physical structure of the vegetation since this information is to be used for the calculation of the hydraulic roughness[1].

The combination of CASI (spectral information of pixels) and LiDAR (height information of points) is expected to improve the result of the classification because they could complement each other.

However, the combination of the two images can bring some difficulties due to the respective different kind of data and hence the information they provide.

Considering that the LiDAR image consists only in points (x, y and z coordinates), one of the main challenges of this study is to transform these points into an image that can be used to discriminate vegetation classes.

Once this problem is overcome, the last step would be to find a straightforward approach to combine both images.

1.3 Objectives

The main goal of this research is to perform a classification of vegetation (according to structural classes) combining the CASI and the LiDAR images.

For this purpose the following objectives have been set:

- Develop a methodology to extract as much information as possible from the LiDAR image trying different statistical approaches.
- Develop a methodology to combine (fuse) the CASI and the LiDAR images in the same classification procedure.
- To assess the accuracy of the different approaches (single and fused images) with the help of ground truth data.
- Try different types of classification methods: *Maximum likelihood* and *classification tree analysis* for the fused image.

---

1 Hydraulic roughness is an index very difficult to calculate. It depends on many different factors like vegetation height, density and stem diameter, but also on pattern distribution of the vegetation clusters or angle of the clusters according to current direction, among others (Asselman, 2001). The calculation of all those parameters is beyond the scope of this study, which would include a much deeper and broader study, including complicated spatial statistics analysis techniques and the support of much more complete and detailed ground truth information. However, since the discrimination of the different vegetation structural classes is one of the most important parameters in determining the hydraulic roughness, this objective will be aimed at in this study.

1.4 Research questions

This research is mainly expected to answer the following questions:

- Which **extra-information** do we get with the fusion of the two datasets?
- Which **statistical methods** and **searching area** sizes are more appropriate to discriminate features from the LIDAR images?
- Which approach gives the **best classification accuracy** for our study case?

1.5 Set-up of the report

From this point on, the report is organized as follows: Chapter 2 involves three parts, the first gives an overview about data fusion levels, then the main characteristics of the two data sets that are used for this study, the CASI and the LiDAR images, are described and finally there is a description of different approaches to fuse both images. Chapter 3 describes and explains the materials and the methodology developed for this study. In Chapter 4 the results of the research are shown and discussed. The report ends with the final conclusions and a list of recommendations for further studies (Chapter 5).

2 Fusion of CASI & LiDAR

This chapter starts with a brief overview about the concept of data fusion and the different levels at which data fusion can take place. This is followed by a more or less detailed description of the characteristics and possibilities of the two types of datasets used for this study, the hyperspectral imagery (CASI) and the laser scanning (LiDAR). After the description of the two datasets, a review of the different approaches found to fuse CASI and LiDAR data is addressed. The literature found about this specific subject is not abundant, mainly because the application of LiDAR has been used vastly for different studies only in the last few years. Also the regular use of hyperspectral sensors like CASI is relatively recent, so it is not strange that there is not much done till now on the fusion of hyperspectral and laser scanning data.

However, the idea of integrating these two sensors is quite promising, even more since the two sensors can be complementary to each other, providing each one of them exclusive information that can lead to a better discrimination of the ground features under investigation.

2.1 Data fusion

During the last years data fusion has become an important issue in remote sensing image analysis. Image analysts can benefit from the fact that different sources and kind of images can give more and higher quality information than one single data source.

From this idea we could say that the overall goal of data fusion (although there is a great controversy about this concept) is to obtain "interpretations of a higher quality when compared to interpretations derived from a subset of information sources' (Hahn and Baltsavias, 1998).

This definition emphasizes on the quality, although the exact definition of quality depends upon the application.

A more simple definition and straightforward definition is "image fusion is the combination of two or more different images to form a new image by using certain algorithm" (Pohl and Van Genderen, 1998).

In the case of image classification fusion of different sources would aim to improve the visual interpretability or class discrimination.

Image fusion can take place at three different levels: pixel, attribute/feature and decision level. The selection of the level depends on the type of data and the output required (Muhammad, 2002).

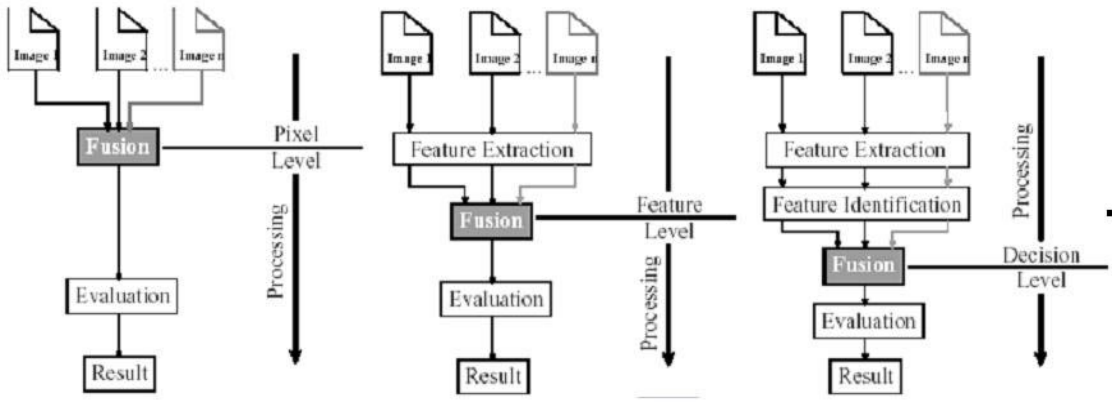

Fig. 2: Fusion levels. From left to right: Pixel, feature/attribute and decision levels

2.1.1 Signal/pixel level

The fusion at pixel level takes place before the features are extracted from the images. It can be said that it is a fusion at 'raw' level. This level of fusion is utilized in the case that the measurements are commensurate or sufficiently correlated. This level of fusion is mainly used for earth observation system's raw data.

The main characteristics of fusion at pixel level are:

- Minimum information loss
- Decision making consists of interaction between users and data sets
- Fusion of only similar and complementary data sensors
- Measurement driven process
- The context information might be non-existent to determine the link of an identified entity with a real world.

2.1.2 Attribute/feature level

Fusion at attribute or feature level requires first the extraction of the representative features from each image. Then the information coming from these features is fused. The main characteristics of feature level fusion are:

- Large dimensions of feature vector

- Decision making consists of interactions between users and feature data
- Allow the fusion of data from non-similar sources
- Evidence-driven process
- Allow general level of uncertainty

This level of fusion is mostly used to derive secondary data like vegetation indices, texture, slope, land cover, aspect.

2.1.3 Decision level

When the fusion takes place at decision level, the attributes of the entities under investigation have already been identified before fusing the information (by classification of the images).

The information extracted from the individual images is combined using some prior probabilities based on the understanding of the features that are being analyzed.

This fusion level is usually applied to complex structured data like environmental processes.

The main characteristics of this fusion level are:

- Complex data sets can be fused
- Knowledge process based on decisions and criteria constraints
- Allow the fusion of non-similar sources
- Model driven process
- Allow different abstraction levels in space and time.

2.2 Multispectral image (CASI)

One of the most recent breakthroughs in remote sensing has been the development of hyperspectral sensors and the software to analyze the resulting image data. Hyperspectral airborne sensors are being used for multiple disciplines with great success, combining some of the better characteristics of aerial photography and satellite imagery with the analytical potential of a spectrometer (*http://www.itres.com/docs/casi2.html*)

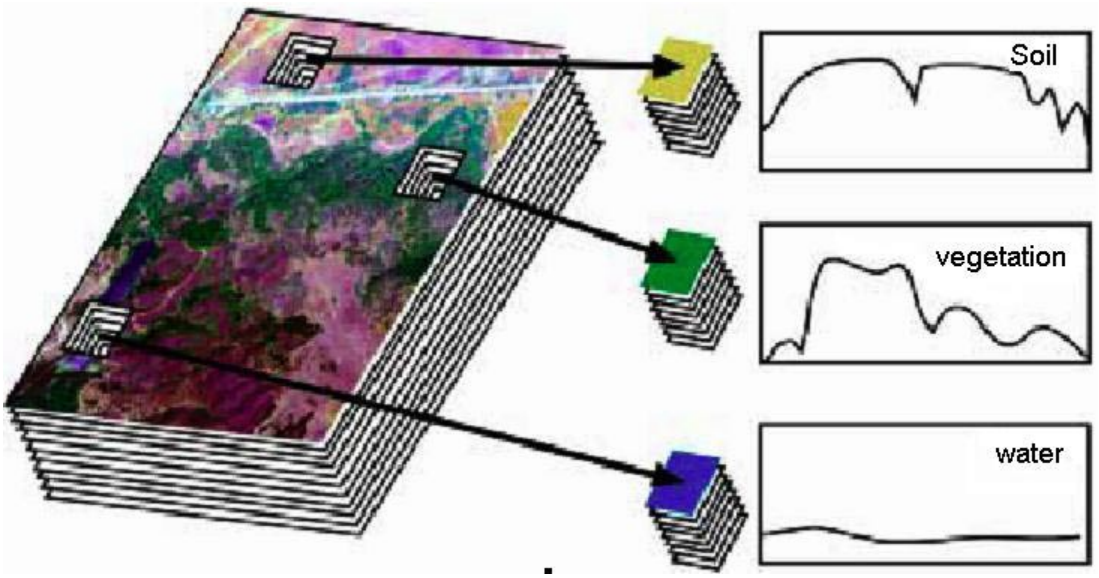

Fig. 3: The concept of hyperspectral imagery. Image measurements are made at many narrow contiguous wavelength bands

Hyperspectral sensors are one type of a remote sensing instrument that can collect several hundred spectral bands of data at a high-spatial resolution. These sensors are generally airborne sensors. Data are collected at contiguous, narrow band wavelengths for a specifically-defined portion of the electromagnetic spectrum.

The **Compact Airborne Spectrographic Imager (CASI)** has been in commercial production since 1989. This hyperspectral sensor detects a vast array of narrow spectral bands in the visible and infrared wavelengths, using along-track scanning. The spectral range covered by the 288 channels is between 0.4 and 0.9 µm. Each band covers a wavelength range of 0.018 µm. While the spatial resolution depends on the altitude of the aircraft, the spectral bands measured and the bandwidths used are all programmable to meet the user's specifications and requirements. However, only a maximum of 15 bands can be used in each measurement. For that reason this sensor is also referred to as 'multispectral'.

Hyperspectral sensors, such as this, can be important sources of diagnostic information about a specific target's absorption and reflection characteristics, in effect providing a spectral "fingerprint".

Traditionally, the sensor has been used to identify and map geologic features, such as mineral deposits (Shang *et al.*, 1999). However, there are many other applications of these data. Some of these applications include:

- Mapping and classification of wetland vegetation (Von Hansen and Sties, 2000)
- Delineate and classification of plant communities (Kurnatowska, 1998)
- Identifying specific agricultural crops (Protz *et al.*, 1999)
- Mapping bathymetry in near-shore environments (Smith *et al.*, 2000)
- Coastal wetland mapping (Shang *et al.*, 1998)
- Identifying forest structure and composition (Gong *et al.*, 1995)
- Identifying soil parameters like soil moisture, organic matter, iron oxide, particle size and soil color (Skidmore *at al.*, 1997).

Thus, due to the capability of measurements of the reflected radiation at a series of narrow and contiguous wavelength bands, CASI (and other hyperspectral sensors) provides the potential for more accurate and detailed information than other types of remotely sensed data.

2.3 Airborne Laser Scanning (ALS)

The development of the airborne laser scanning goes back to the 1970s and 1980s with an early NASA system and other attempts in the USA and Canada (Ackermann, 1999). Then, thanks to the solution that the DGPS provided for the positioning problem, high accuracy performance became feasible and the application of this system became rapidly more and more in extended use.
The Airborne Laser Scanners (**ALS**) are also called **LiDAR** (Light Detection And Ranging) or **LADAR** (Laser Detection and Ranging), referring to the fact that the light used by these devices is a laser.

2.3.1 Principles of laser scanning

The scanning system measures the distance between the sensor and the spot on the ground that is illuminated. For each shot that goes from the transmitter and comes back to the optical receiver, the spatial vector from the laser platform to the point of reflection is calculated.

This calculation is based on the measurement of the time that the laser beam takes to go from the scanner, hit the ground object and return to the sensor. Basically, the traveling time (t_L) of the laser bean would be:

$$t_L = 2\frac{R}{c}$$

where R is the distance between the scanner and the ground object and c is the speed of light. So the distance from the sensor to the ground object can be derived as follows:

$$R = \frac{1}{2} c \cdot t_L$$

However, the laser scanner measures only the vector from the airborne platform to the ground. So, a ground reference is necessitated if we want to transform these coordinates into ground coordinates. For this purpose, the laser scanner system must be supported by a POS (Position Orientation System). The laser scanners have a potential accuracy of better than 0,1 m (Wehr and Lohr, 1999), so the ground support system should allow at least the same. This can be achieved only by an integrated POS consisting of a DGPS and an IMU (Inertial Measurement Unit). So, collecting the laser measurements requires a perfect synchronization of all these three systems: laser scanner, DGPS and IMU.

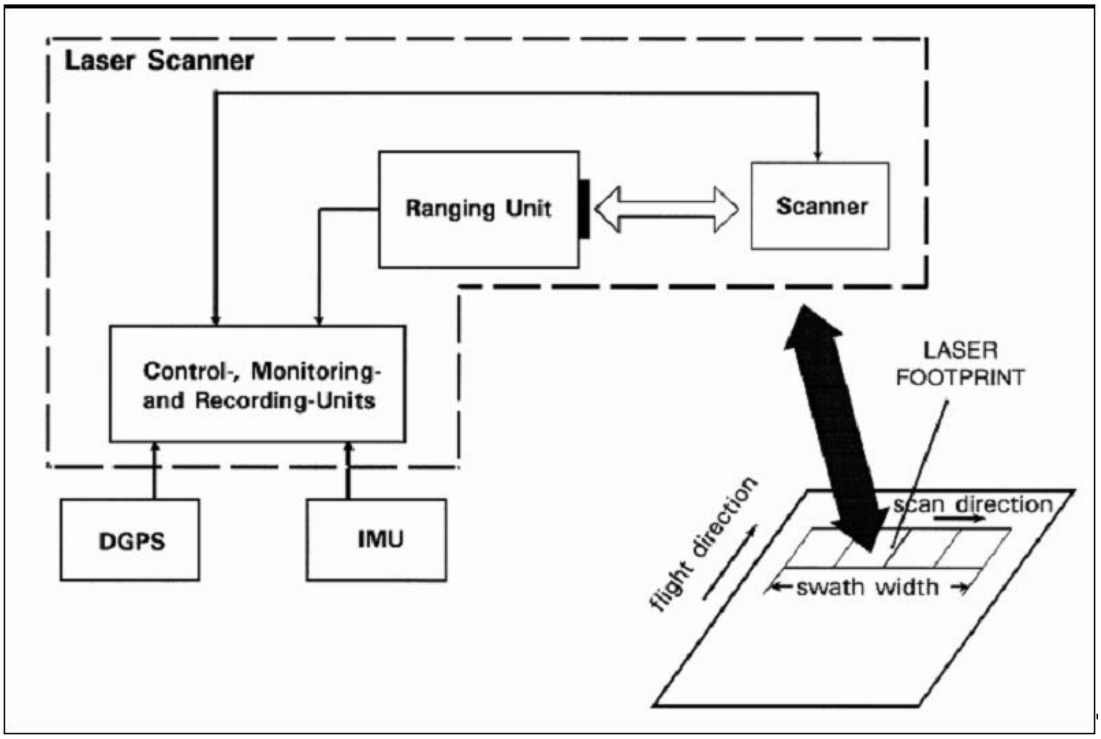

Fig. 4: Typical airborne laser scanning system (From Wehr and Lohr, 1999)

The laser operates at **frequencies** that can vary from 800 till 1600 nm. This is an important factor to take into consideration because different materials have different reflectivities depending on the wavelength. The reflectivity will determine then the maximum range of the system (according to minimum percentage of reflection that the receiver can register). So, depending on the type of feature that we would like to study, the wavelength of the laser could be a factor to take into consideration.
Based on the backscattering properties of the targets, different scanning systems have been developed than can be used for several purposes. For instance the SHOALS system, that is used for bathymetry measurements, can register altitudes of the water surface and water floor at the same time. This is achieved combining two wavelengths: Infrared, which reflects on the water surface, and blue-green, which penetrates the water and reflects on the bottom. In this way depths up to 50 meters (in clear water) can be measured.

The **intensity** reflected by the object can also be registered by some scanner systems. This information can be used as a 'mocromatic' band that can add information to the laser image. For example, Asselman (2001) used the intensity records for reconstruction of vegetation patterns in a floodplain. This is an important feature to take into consideration if we consider the 'blindness' of the laser image about the capture and identification of objects. This concept of blindness means that the information given by the laser image is only structural and necessitates additional image information in order to have a better understanding of the features under study. This information can be provided by the measurement of the intensity of the laser signal (as mentioned before) or by the combination with a different data set, like multi or hyperspectral imagery.
In fact, efforts are being put in integrating two sensors in the same platform sharing the same POS. In this way the geometrical match between the two data sets would be the best. The next step would be an automatic merging of the information in such a way that the two images would be completely integrated. This complete integration could mean a complete revolution in remote sensing analysis (Ackermann, 1999).

The **spatial resolution** of the laser scanning is one of the most important characteristics of this system. The density of the laser points can range from one point per 20 m^2 up to 20 points per square meter. This density depends principally on the balance between the type of scanner (scan frequency and repetition rate) and

the flying speed and the altitude of the aircraft. The geometric sampling pattern on the ground is predetermined by the setting of the sensor, although the 3-D structure of the terrain has some influence.

The **footprint size** (diameter of the laser beam when it hits the surface) is another variable of this system. It depends on the type of sensor (aperture angle of the transmitter) and on the flying altitude. The size of the footprint can vary and depends on the purpose. Some systems use large footprint systems like the SLICER (Means *et al.*, 1998) or LVIS (Blair *et al.*, 1999), which use footprint sizes of up to 30 meters diameter. Other systems utilize small footprints, like the ALTM sensors with footprint sizes of 15-30 cm diameter.

The laser pulse, after hitting a morphologically complex surface such as a vegetation canopy, will be a complex combination of different responses returned from numerous distances.
The type of information collected from this return signal distinguishes two broad categories of sensors **discrete-return** and **waveform-recording devices** (Lefsky *et al.*, 2002).

The **discrete-return devices** measure either one or a small number of heights, normally first and/or last significant returns. These systems usually work with a small footprint size (15-30 cm) and at a very high pulse rate, allowing a very high spatial resolution, and densities up to several points per square meter. Discrete-return systems are preferred for detailed mapping of the ground and generation of accurate DTM's (Flood and Gutelius, 1997).

Waveform-recording devices record the whole time-varying intensity of the returned energy for each laser pulse, from the first to the last return. These systems have the advantage of being able to characterize canopy structure over large areas. These devices normally work with a large footprint size and are capable of collecting more information on canopy structure than the discrete-return devices. Several studies have been carried out with this type of sensor to estimate vegetation characterization (Means *et al.*, 1999; Blair *et al.*, 1999). Moreover, only waveform recording will be collected globally from space in the near future (Lefsky *et al.*, 2002).

The waveform-recording devices are used mostly for research purposes, although they are not as widely in use as the discrete-return LiDAR systems (small footprint & high pulse rate), which are nowadays used vastly for commercial purposes. The availability of data of the latter is larger. Hence, this overview about the LiDAR applications and properties will focus more on the use of small footprint-discrete return devices.

In figure 5, the principles of discrete and waveform-recording systems are described (from Lefsky *et al.*, 2002).

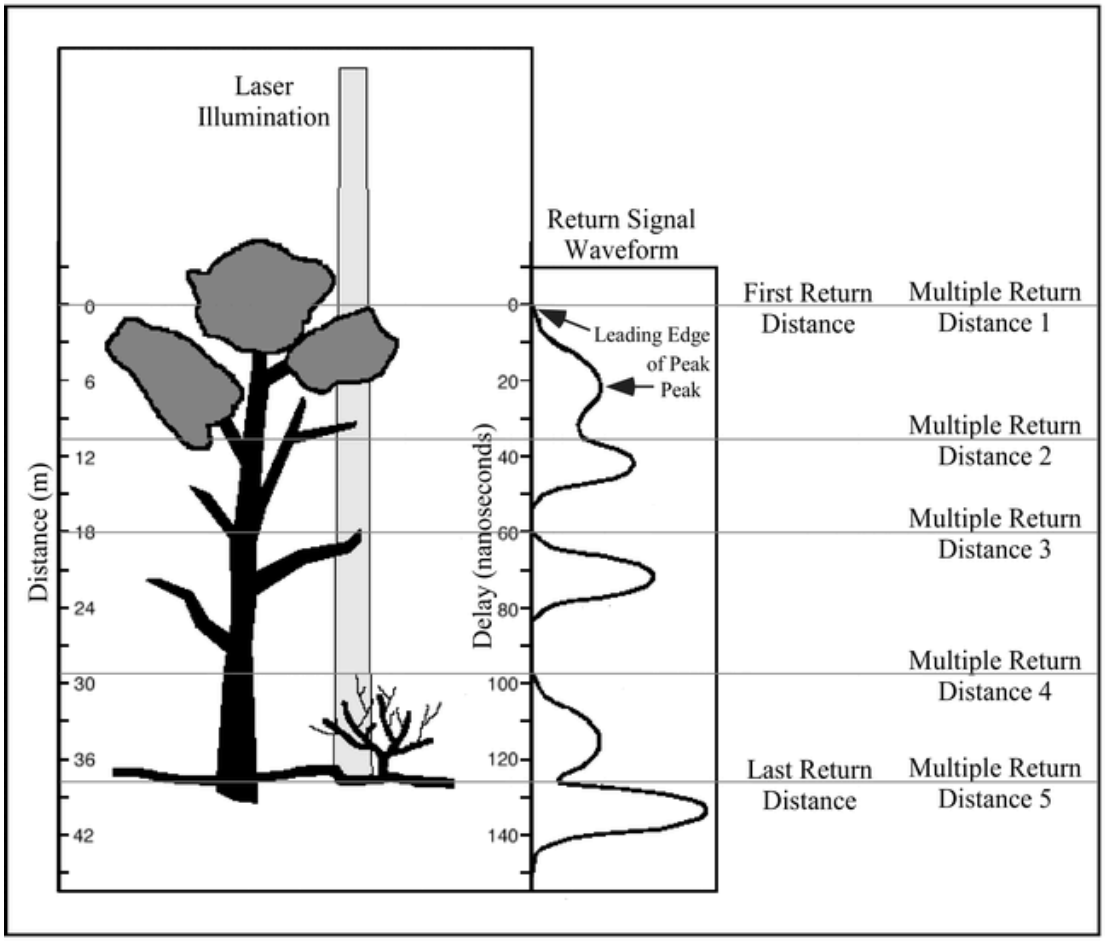

Fig. 5: Conceptual differences between waveform and discrete-return devices

In the case of a regular surface, like ground, the return of the pulse is unique, but when it hits irregular objects like vegetation, the return signal will be multiple. As mentioned before, some systems can record multiple responses. Among this type of

sensor, the most common are the scanners that are able to register the **first and the last pulse** for each height point. As a result of that, two different heights in one point gives an indication of the presence of a penetrable object, such as a tree. This very important information can be used to discriminate features on the ground. A unique response would reveal the presence of a solid object, like ground or a flat roof of a building, whereas two different heights would show a penetrable object like a tree.
Studying the kind of response in areas covered by vegetation, characterization of vegetation types can be carried out based on the structure of the plants.

One of the most important applications of ALS is the **generation of Digital Terrain Models (DTM)** in conditions where other systems like photogrammetry or ground surveying find some difficulties, for instance in terrain with vegetation cover, coastal areas or wetlands (Ackermann, 1999). This is due to the ability of the laser beam to penetrate the canopy and hit the ground. This potential was the original motivation to study laser systems for the generation of DTM's.
Discrete-return devices with high point density are actually in use for the generation of DTM's and the number of firms providing this service has increased largely in the last years.
The **accuracy** obtained with the DTM's generated from LiDAR and the support of a POS is very high, and usually ranges from 15-20 cm in height accuracy and from 0.3-1 meter in planimetric accuracy (Baltsavias, 1999).
Although the complete cost of a LiDAR survey is important, the ratio 'price/high accuracy point' that laser scanning offers is quite low compared to other systems of generating DTM's (http://www.optech.on.ca/).

For all these characteristics, the ALS systems are considered as a powerful source of remotely sensed information and still a lot of effort is being put to extract more information from these data sets.

2.3.2 Applications and special characteristics of the ALS

Since the beginning of the use of the ALS systems several fields have received benefit from the special properties of this sensor. The most important fields in which this technique has been utilized are:

- Generation of accurate DTM's (http://www.optech.on.ca/)
- Estimation of individual canopy height (Nilsson, 1996)
- Characterization of canopy structure (Lefsky *et al.*, 1999)
- Determination of volume of timber (Naesset, 1997)
- Bathymetry surveying (Irish *et al.*, 2000)
- 3D modeling of urban areas and extraction of urban features (Alharthy and Bethel, 2002)
- Land cover classification (Song *et al.*, 2002)
- River flood modeling (Cobby *et al.*, 2001).

The most important characteristics of the ALS system can be summarized as follows:

- **High-resolution**, up to several height points per square meter.
- High-accuracy digital elevation data. Depending on the sensor, up to 10-15 cm in height and 30 cm planimetric.
- Unaffected by poor contrast - Some areas such as mud flats or beaches have poor optical contrast making photogrammetry difficult or impossible.
- Independent of lighting conditions – Since it is an active sensor system, it is not affected by lighting conditions. Acquisition can take place with overcast sky and at night, as long as there are no clouds between the aircraft and the ground.
- Range measurements independent of target composition: Bright targets such as sand or snow give the same range as dark targets such as asphalt.
- Vegetation penetration - Ground elevations can be obtained even in dense forest cover due to the ability of penetrating the canopy.
- Ranges to trees and to the ground beneath in a single pass - Simultaneous first- and last-pulse capability in the same flight pass.
- **Whole profile signal registration** - For the study of vegetation structure, in the case of the large-footprint waveform devices.
- High Data Rate - A laser scanner can acquire up to 83,000 individually height points per second.

- Fast processing of DTM generation, which can be performed entirely automatically within a short time after acquisition, since all data is digital.

The main disadvantages of the system are:

- Blindness about the capture and identification of objects which leads to modeling assumptions in the data processing. There is no certainty that a laser point belongs to a certain object, for example that the last pulse registered for one point comes from a ground hit. This problem can be overcome partially with the addition of extra information like the recording of the reflectivity of the laser signal or the combination with other data sets.
- Storage and manipulation difficulties due to the large size of the datasets. This drawback is expected to be overcome with the quick improvement of the hardware and software, which will lead to the possibility of manipulating more and more volume of data.

2.4 Fusion approaches of CASI and LiDAR

There is not much literature about the fusion of hyperspectral and LiDAR data. The two techniques are still under investigation and the fusion of those two data sets is still not widely used. This study focuses on vegetation classification.
Depending also on the aims or the purposes of the classification, the approaches should vary.
After literature review, two approaches were found that could help to make the first steps for the fusion of LiDAR and CASI.
First, an analysis of how information can be extracted from ALS data and then a description of two approaches to combine this information with CASI is given.

2.4.1 First step: Texture Analysis of the LiDAR

Texture represents local variations in the spatial domain and determines the overall visual smoothness or coarseness of image features (Lillesand and Kiefer, 2000).

The local variation of the LiDAR data can be used to analyze the data. The texture as expression of local variation is used by the human eye to distinguish different

objects, although it is not easy to establish an objective model to describe this intuitive concept (see figure 6). The texture can be defined by means of different statistical parameters or with more complex techniques, analyzing more deeply the spatial variability patterns of each class with the use of variograms (Miranda *et al.*, 1998).

Analyzing the texture is, in fact, not a new approach. It is not exclusive for altimetry and it has been used with radar and traditional imagery data. Haack and Bechdol (2000) examined the utility of radar to locate areas of natural vegetation using measures of the texture of the image by means of several statistical approaches. Chica-Olmo and Abarca-Hernandez (2000) improved classification in lithological studies by adding texture information as extra layers to a Landstat-5 TM image. In that study, a 'pixel- based' variogram analysis was carried out to obtain different extra 'texture bands'.

Texture has also been analyzed in LiDAR images. Maas (1999) analyzed the texture of the LiDAR data to automatically detect different features types in urban areas.

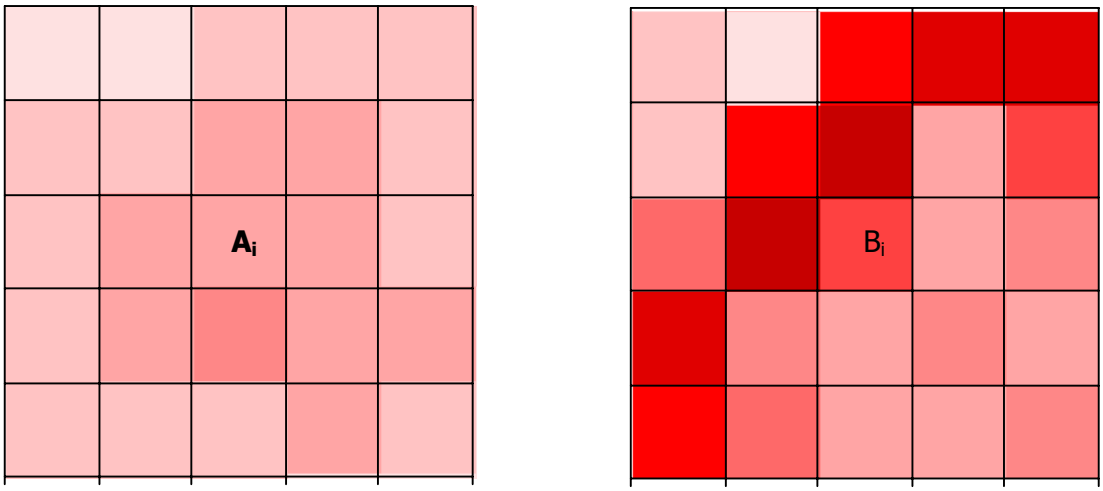

Fig. 6: Concept of texture analysis: Values can be assigned to pixels A_i and B_i analyzing the variability according to the neighboring pixels. If these two figures belonged to different classes, the pixels A_i and B_i could be classified looking at the different spatial pattern behaviors. This concept can be applied for reflectance values as well as for altimetry data.

Getting a bit more into the technical part, the problem of analyzing the texture in LiDAR data comes from the fact that the original LiDAR points have an irregular distribution. Till now, most of the approaches first converted the LiDAR points into a

regular grid by means of interpolation techniques (Hill *et al.*, 2002), and then analyze the texture using filters that calculate different statistical parameters (Maas, 1999). However, Axelsson (1999) recommended that all processing of LiDAR data should be done without sampling firstly the data into a regular grid, because during this process there is a loss of information. This research tries to avoid this problem by using the raw LiDAR data to derive the statistics.

An other important source of information to analyze texture (and unique of this system) is the multiple return sign for each point that many laser scanning systems can provide (first-last return or waveform scanners). The analysis of this data can be used together as extra information for texture analysis.

Once the texture is transformed into values, it can be assigned to pixels, and this information is then utilized as a 'texture' band for further analysis.

2.4.2 Pixel level

Maas (1999) and Liapis *et al.* (1997) used the texture of a LiDAR image as 'bands' in the Maximum Likelihood Classifier. Based on the principles of this classification technique it is possible to add different 'texture bands' to this classifier. The same procedure could be applied to other classifiers like neural networks or decision tree analysis.
At this point of the analysis it would be feasible to incorporate extra spectral information from other sensors, like CASI or other sensors. The combination of these two completely different sources of data can be a revolution in remote sensing analysis.

The main advantage of this approach is the fast calculation and the simplicity of the procedure. Once the texture information of the LiDAR image is transformed into pixel values with the same spatial resolution as the CASI image, the only thing we have to do is to input all the different layers into the classifier.
At this point we should take into consideration that the scale of the two data sets has to be the same when we use Maximum Likelihood Classification. Here, the point of controversy is whether two completely different types of information (reflectance and texture or altimetry) can be set into the same scale. However, assuming that the

texture information of each class can behave as a normal distributed variable, it should not be a problem to incorporate texture bands into the Maximum Likelihood classifier.
In any case, this controversy could be overcome with the use of classifiers that do not need rescaling of the data, like the *classification tree analysis,* that can work with multiple bands independently of the scale and even with categorical variables.

The main disadvantage of the pixel level approach is the lack of information concerning the classification decisions made by the classifier. A deep understanding of the functioning is needed to understand which is the influence of the different bands in the classification. However, some classifiers like the neural networks and the decision tree analysis, provide information about the weight of each band in the classification procedure. Though, even with this information, mixing all these bands at pixel level is still a rather 'black box' approach, which gives little information about the classification procedure.

2.4.3 Feature level classification

In this case, the first step would be the same as the one explained in the previous section. The texture and other measurements must be derived firstly from the LiDAR image. Afterwards, instead of inputting all the obtained layers plus the CASI layers into one classifier, the classification would be carried out following different steps.
Based on expert knowledge or on empirical approaches, the best layers to classify each class can be determined and used to classify and mask step by step the different classes. Maybe with an example it can be explained clearer.
Let's assume that we use LiDAR and CASI to classify four types of cover types: *bare soil*, *grass*, *bushes* and *forest*. Based on previous knowledge, we could assume that the CASI will distinguish better than the LiDAR between *grass* and *bare soil* because the spectral signature is quite different, whereas LiDAR would find problems to discriminate those two classes. However, when the classes *bush* and *forest* have to be classified, the LiDAR could be a better solution to discriminate them because the physical structure of the two classes is different. Thus, in this case we could use first CASI to classify and mask out the *bare soil* and the *grass* from the rest of the image. Later on, only the LiDAR would be used to classify the other two classes, *bushes* and *forest*.

The main advantage is that in this way we avoid the 'black box effect' of the classifiers and moreover we avoid the noisy information that some layers, which are confusing to discriminate some classes, can cause. The effect of the noisy layers and the confusion they can produce in the classification is not clear for some classifiers.

On the other hand, this method is not as straightforward as the pixel level approach and moreover it requires expert knowledge in order to select the classes that will be discriminated with each image.

3 Materials and research methodology

This chapter describes the materials used and the methodology developed to combine the CASI and the LiDAR images and perform the final classification.

The approach followed for this study was a straightforward one, since the river manager was demanding a direct method to classify vegetation in the floodplains, thus fusion at pixel level was chosen. As explained in the previous chapter, to achieve this, the texture and other measurements must be derived from the LiDAR image, before fusing with the CASI and performing the classification.

In our case the first inconvenience we had to overcome was that the two images, CASI and LiDAR give a completely different type of information: spectral response and 3D structure, respectively. Moreover, the CASI provides information for pixels in a continuous grid, whereas LiDAR provides point wise information in an irregular pattern. All procedures are described in this chapter.

In the flowchart of figure 7 the methodology is shown. It aims to explain in general terms the most important steps followed.

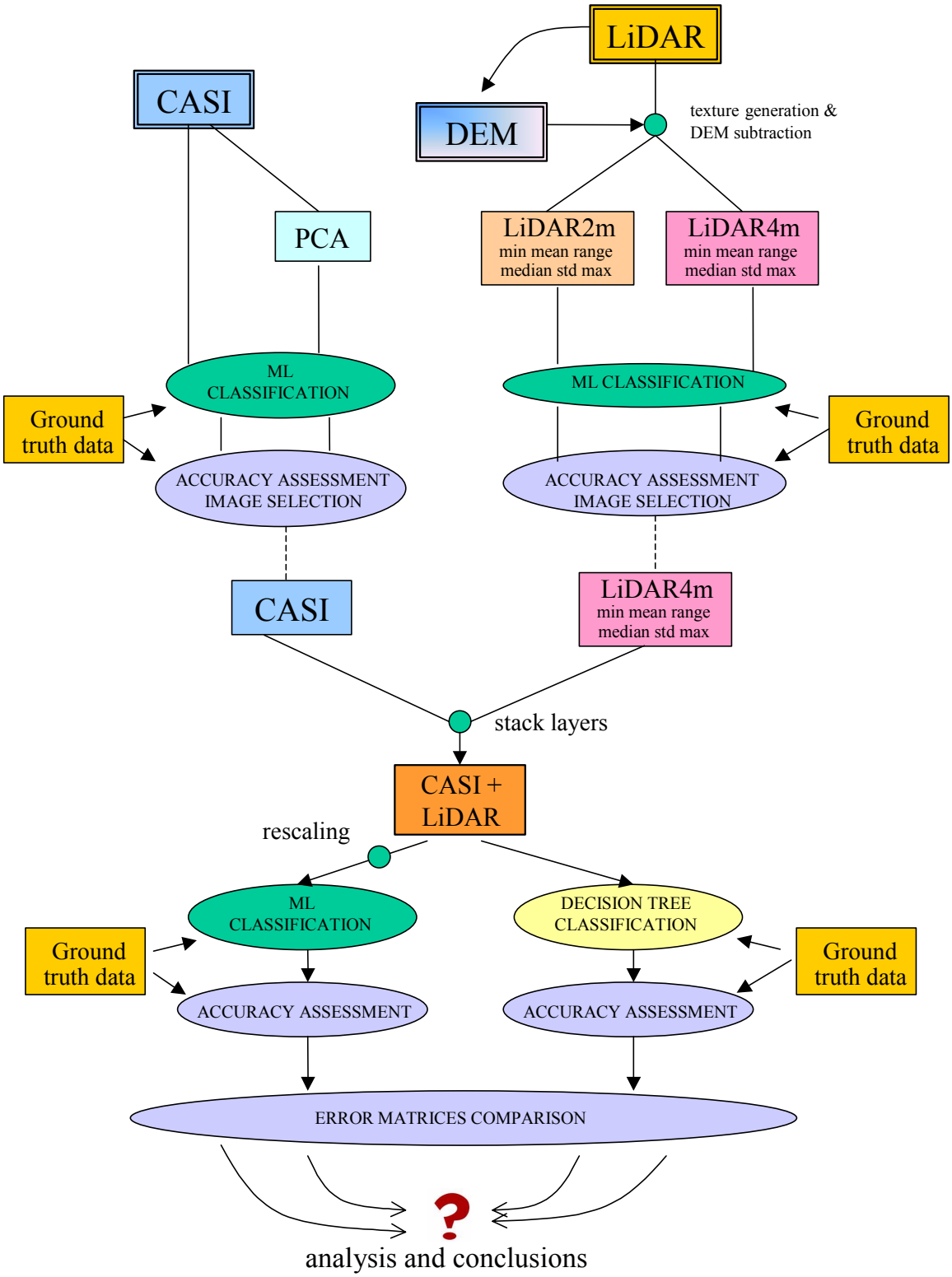

Fig. 7: Methodology of the current study

3.1 Ground truth

As mentioned in the introductory chapter, the aim of this research was to classify vegetation according to structural classes. The ground truth of this research is based on a study in the same area carried out by two students of Wageningen University. The vegetation classes were chosen according to their physical structure.
In the original study 24 ecological classes were defined based on ecological communities (classes) in the floodplain. These 24 classes were regrouped in 7 classes, which were defined in relation to their influence on hydraulic roughness.

A total of 334 plots were available for classification and accuracy assessment, representing 8 classes. The ground truth plots of the class 8 (forest) were obtained by visual interpretation of the LiDAR image, in which the forest is clearly represented.
The ground truth plots of classes 1 to 7 were approximately 3x3 meters and for each plot an exhaustive analysis of the existing vegetation types was done. From this study, the structural classes were derived and assigned to each plot.
The structural distribution of the vegetation classes (except for class 8 –forest) is shown in the appendices in detail. However, for better understanding of this chapter and the results and conclusions, a brief description of the 8 classes can be summarized as follows:

Class 1: *Sandy bare soil, with a unique spectral response.*
From class 2 to 6*: Different plant communities, aggregated according to their structural class, gradually increasing their height from class 2 until class 6.*
Class 7: *Small community of tall bushes.*
Class 8: *Large forested area, spectrally and mainly structurally very different to the rest of the classes.*

Figure 8 shows the approximate average vegetation height of each one of the eight classes.

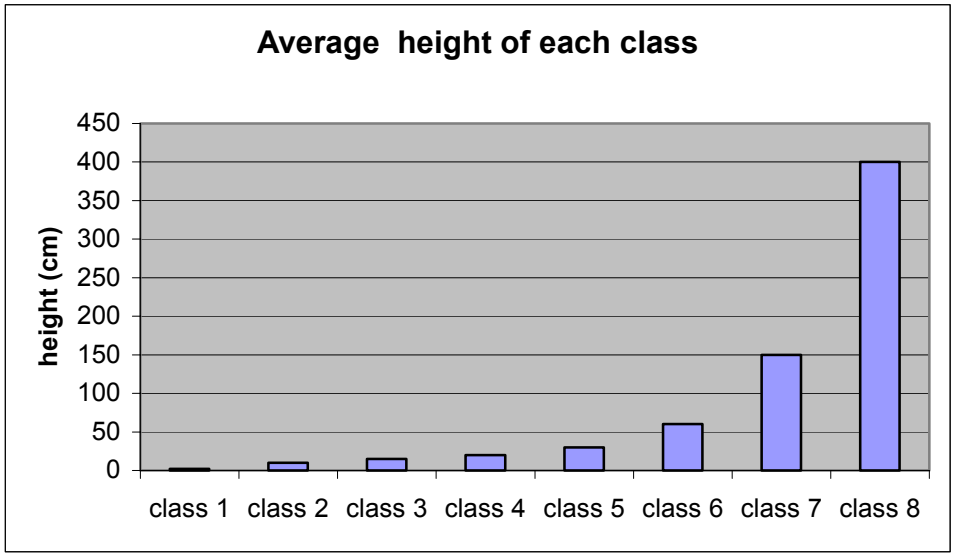

Fig. 8: Average height per class

Half of the plots of each of the 24 subclasses (subsequently of the 8 classes) was used for training and the other half was used for the accuracy assessment. The selection of the plots for training and accuracy assessment was made randomly within each class.

3.2 Preprocessing of the images

3.2.1 CASI

The Compact Airborne Spectrographic Imager **(CASI)** is an airborne hyperspectral sensor of 288 narrow bands of 1.8 nm of interval, between 400 and 915 nm. For this study 10 bands were available:

Band	Wavelength (nm)	Colour
1	437 – 447	Blue
2	549 – 559	Green
3	615 – 625	Red
4	671 – 680	Red
5	681 – 689	Red
6	695 – 705	Red
7	729 – 739	Near-IR
8	757 – 767	Near-IR
9	860 – 867	Near-IR
10	880 – 890	Near-IR

Table 1: CASI spectral bands

The image was taken on 15th Augustus 2001. The spatial resolution of the CASI image was 2 x 2 m per pixel.

The image did not need atmospheric correction since we were not using multitemporal analysis and only performing image classification. Thus the image was almost ready for its analysis. Two images, which covered the whole study area, were overlapped and mosaiced together. Then an AOI was used to mask the study area (figure 9).

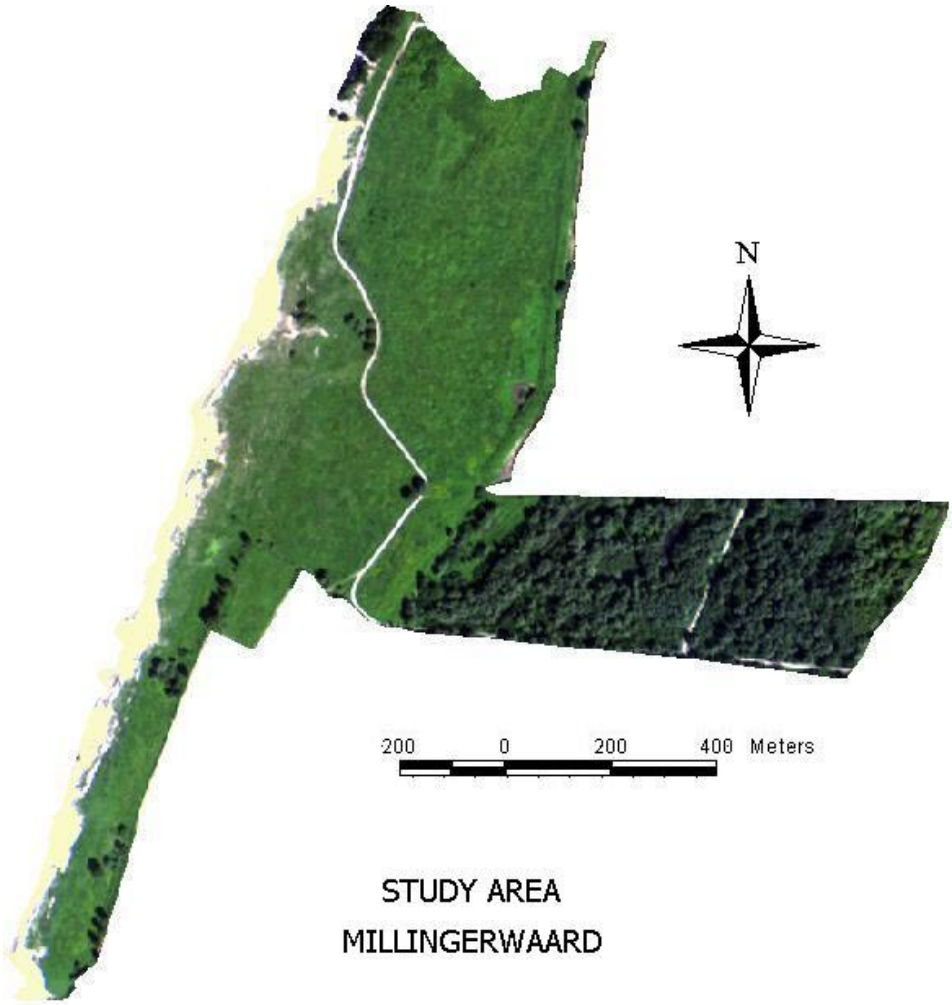

Fig. 9: Study area, the *Millingerwaard*.
CASI image: composite true color bands 1, 2, 3 (blue, green, red)

3.2.1.1 Principal component analysis (PCA)

In order to reduce the dimensionality of the CASI image and avoid possible redundant information coming from correlated bands, a Principal Components technique was applied to the CASI image. Principal components analysis basically creates different bands as linear combinations of the original bands. The principal components are generated in such a way that the first one expresses the maximum variance, whereas the rest account for less and less variability. Normally most of the total variability is concentrated in the first 3 or 4 principal components. That means an effective way of reducing the dimensionality of the dataset, which can increase the computational efficiency of the classification process (Lillesand and Kiefer, 2000)
The principal component analysis was performed and the first four PC were merged in a new image that was used for further analysis. The first four principal components explained 99.96 percent of the total variance (table 2).

Principal component	% of the total variance
pc1	94.07%
pc2	5.73%
pc3	0.12%
pc4	0.04%
total	99.96%

Table 2: Variance percentage of each principal component

3.2.2 LiDAR

The LiDAR image was provided in the form of an ASCII file with xyz coordinates. It had to be transformed into an ArcInfo® point coverage, so that the manipulation with the existing software was possible. The spatial pattern of the LiDAR points was semi-regularly distributed with a density of about 1 point per square meter. However, the point density was not constant. This fact will be analyzed further on in this chapter. Only first-return pulses were available for this study.

The date of the flight was the 12th October 2001. The type of scanner was the **ALTM 2033**, developed by Optech (www.optech.on.ca). The most important specifications of the flight surveying were:

- Flight altitude: about 800 m
- Repetition rate of the laser pulse: 33 kHz
- Scan frequency of the mirror: 30 Hz
- Scan angle: 19 degree.

During the surveying, three terrestrial measured reference fields were used to estimate the LiDAR error. In each of these ground control fields about 100 terrestrial measured points were lying. The result was:

- Height error: approx. 15 cm
- Planimetric error: approx. 50 cm.

3.2.2.1 LiDAR pre-processing

As mentioned before, the spatial resolution of the two images has to be the same. For that reason, the first logical approach was to bring the spatial resolution of the LiDAR into the CASI's, which is 2 x 2 meters/pixel.
Since the information that the LiDAR image gives contains only *xyz* coordinate points, the image had to be transformed so it can be analyzed at pixel level. In this case what can be analyzed is the spatial variation of the height of the points by means of statistical parameters. This information is very useful because it reflects information about the structure of the vegetation.

Several methods to achieve this were considered. One was the transformation of the irregular LiDAR points into a regular grid by means of interpolation techniques and then utilize filters to calculate different spatial parameters (Maas, 1999; Hill, 2002). This method was discarded because, as mentioned in chapter 2.4.1, the interpolation previous to the analysis of the texture creates height assumptions which leads to a loss of information, which is very important for vegetation studies.
Another approach was to overlay a *regular net* over the LiDAR points and derive statistics with the points that fall within each cell of the net. This method, suggested by John Stuiver (personal communication), was also not taken into consideration because of the lack of flexibility and the difficult processes that it required. So, after analyzing '*pros and contras*' of the different approaches, we decided to follow a method that uses the height of the original LiDAR points to derive statistics and apply the result to an output pixel, which size is also predefined by the user.

This procedure was carried out by means of the ArcInfo® command *'pointstats'*.

This method utilizes the height of the original LiDAR points that fall within a predefined search area to derive statistical parameters, which will be assigned to an output pixel, which size is also defined by the user. In this way a grid with texture values is generated for each statistical parameter. In figure 10 this procedure is explained.

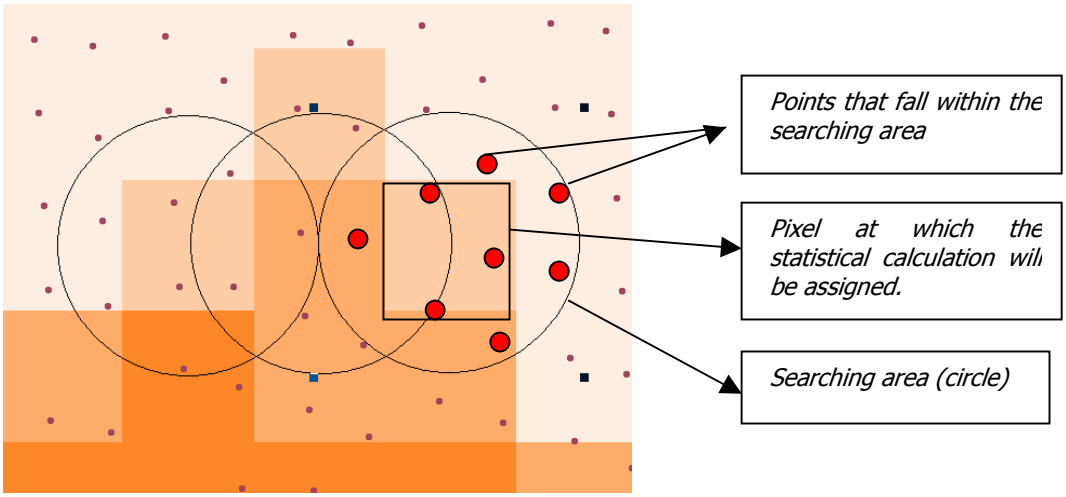

Fig. 10: 'Pointstats' calculation

This method is also very flexible because it gives us the possibility of calculating different statistical parameters and try different search areas for the LiDAR points very easily. The main advantage is that the statistics are derived from the raw LiDAR data and so there is no loss of information during the intermediate transformations. The search area is defined by its shape and extension around each output pixel and it is another variable that can be analyzed.

A model developed in Arisflow® allowed the calculation of many statistical parameters. Several options were chosen in order to find out which LiDAR approach would produce the best classification. An understanding of the vegetation characteristics and how the statistics are calculated from the LiDAR points is needed before trying the different options. Later in this chapter the different approaches to generate LiDAR images will be explained in detail.

The **density** of the LiDAR points was also analyzed. Some patterns that might affect the analysis were found. There are different point densities in different stripes (flight paths) and they change alternatively. Whereas the stripes in one flight direction have a density of approximately 6 points per pixel of 2x2 meters, the other direction has a density of 3 pixels in the same area. Thus, the density of the LiDAR points in one direction is approximately the double of that in the other direction.

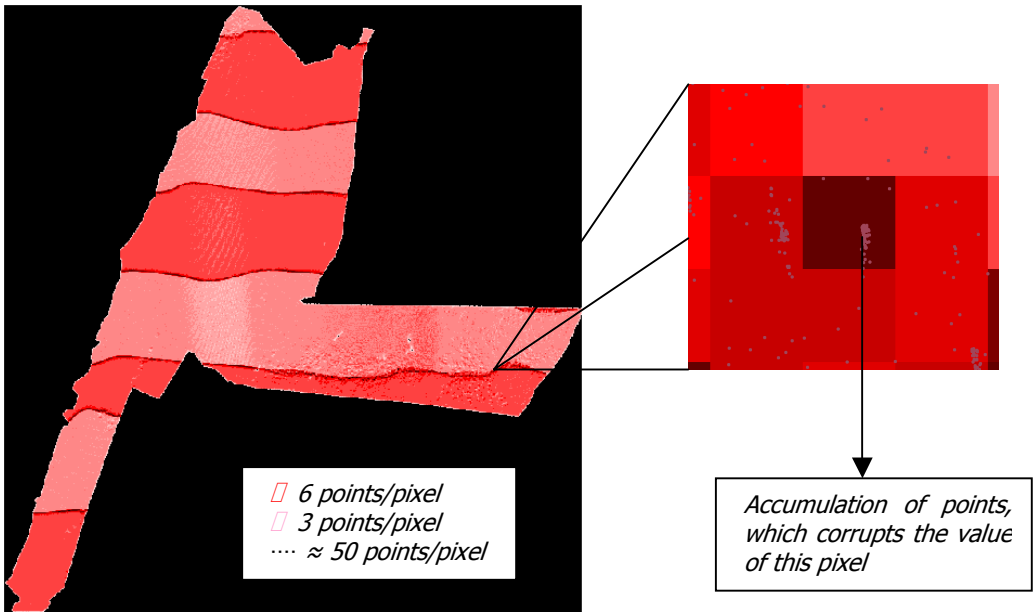

Fig. 11: Accumulation of points at the edge of the swath

Another interesting part of our density analysis was that it was found that there is an accumulation of measurements at the edges of the stripes, at both sides of the flight path. A closer look at the points in these areas showed that the accumulation of points was very high (many times more that 50 points within a pixel of 2x2 meters). The height value of the points has a correct appearance, since they are very similar to the surrounding single points. At first view it was not seen as a problem since it can be considered only as 'extra information'. However, when this accumulation of points falls in the forest, some statistical parameters can give wrong values. For instance, the mean was either too high or too low along these edges in the forest, which ended up showing a line across the forest that resembled a path. Further analysis of the phenomena showed that the accumulation of points produced very high or very low values depending on where the accumulation of

points was situated, usually on the ground or on the top of the trees. The height values of the points forming those clusters were very similar among them.

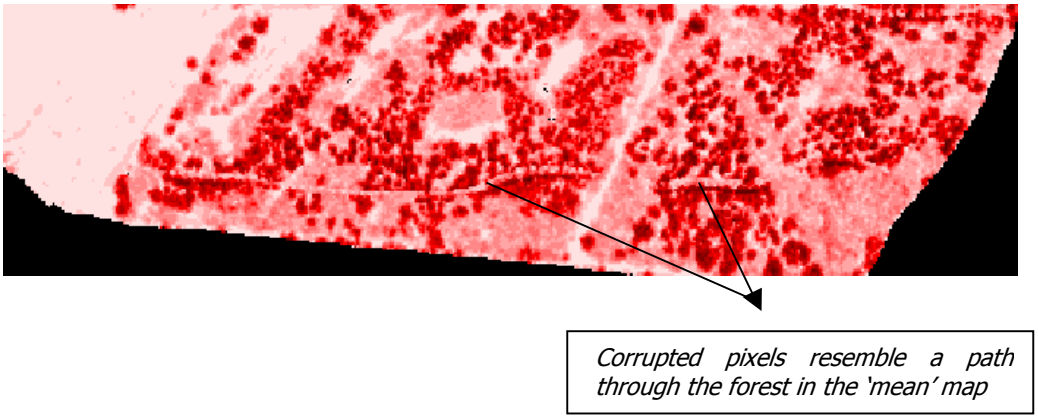

Fig. 12: Image error produced by high point density

3.2.2.2 Statistical parameters

As discussed earlier, several statistical parameters can be calculated and assigned to the cells of the output grid image with this methodology. After considering which information about vegetation structure each one of them could add, six parameters were selected for this research. Other parameters were not taken into consideration because the information added was redundant or not valuable according to our criteria.

MAX *- the maximum z value.*

The output value of the pixel is the maximum z value within the search area.

MEAN *- the mean z value.*

The output value of the pixel is the average z value within the search area.

STD *- the standard deviation of the z values.*

The output value of the pixel is the standard deviation of the z values within the search area.

RANGE *- the range of z values (MAX - MIN).*

The output value of the pixel is the maximum minus the minimum z value within the search area.

MIN *- the minimum z value.*

The output value of the pixel is the minimum z value within the search area.

MEDIAN - *the median z value.*

The output value of the pixel is the median of the z values within the search area.

According to our knowledge, these parameters could add some information that helped to discriminate the different classes according to their physical structure.

3.2.2.3 Image generation

The next approaches were chosen for the LiDAR image in order to see which one gave the best accuracy. The size of the output pixel was set always at 2 meters, the same as CASI:

a) Search area circle 2m radius, 6 bands (min, mean, range, median, std, max)
b) Search area circle 4m radius, 6 bands (min, mean, range, median, std, max).

Other options were tried, like using a search area of the same size as the output pixel (square of 2x2 meters), but the analysis of the grid image showed many 'no-data' points in the forest and also the number of points to derive statistics was very low. Other options like bigger search areas produced too smooth maps where the details were lost and thus were not considered for this study.

3.2.3 DEM

Creating a DEM was necessary in order to avoid the errors of assuming that all the differences of height measures correspond only to variation on vegetation. An accurate DEM was generated using the same LiDAR points. Assuming that many LiDAR beams hit the ground or very low vegetation (like grass), a DEM can be derived using the minimum z value within a certain search area. The bigger the search area, the higher is the possibility that one point falls on the ground, but the worse is the spatial resolution and accuracy of the DEM. Thus, a balance between spatial resolution and reliability that the DEM comes from ground hit points had to be found.

This problem could be avoided if we had used 'last-return' pulses, because then the possibility that one point falls on the ground is much higher and the DEM can be much more accurate, but this data was not available for this study.

Rectangular search areas of 2x2, 4x4, 6x6 and 8x8 meters were tried.

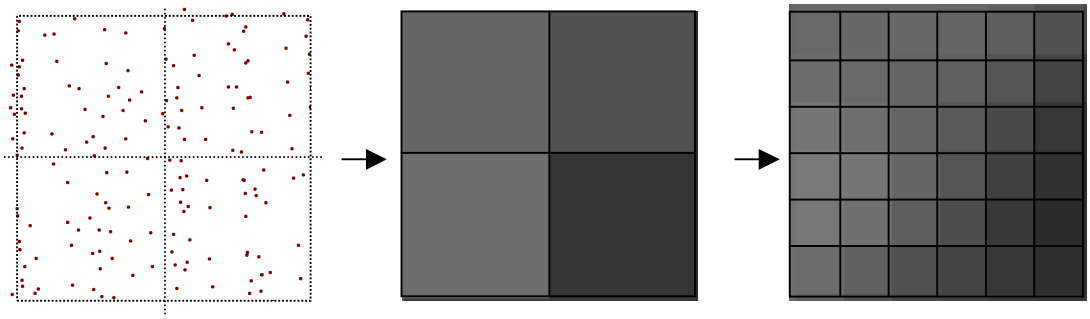

original LiDAR points | *min value assigned to each pixel. DEM of 6x6m.* | *DEM 2x2m after interpolation*

Fig. 13: DEM generation

The best result was given by the 6x6 meters DEM, considering the amount of ground hits and the resolution obtained. In any case, a few points of the 6x6 DEM were clearly not 'ground-hit' points and were corrected manually according to the height value of the surrounding pixels.
The DEM was resampled at 2x2 meters using the 'cubic convolution' interpolator. In this way the DEM had the same spatial resolution as the LiDAR and CASI images and at the same time a kind of interpolation (smoothing) was produced (figure 13).

The DEM was subtracted from the maps where absolute values were represented. Thus, the DEM was subtracted from the 'min', 'max', 'median' and 'mean' maps, and not from the 'range' and 'standard deviation' maps, since they already show relative values, and subtracting the DEM has no significance.
In this way the height information of the LiDAR maps comes only from variation in vegetation height and the effect of the relief is avoided (figure 14).

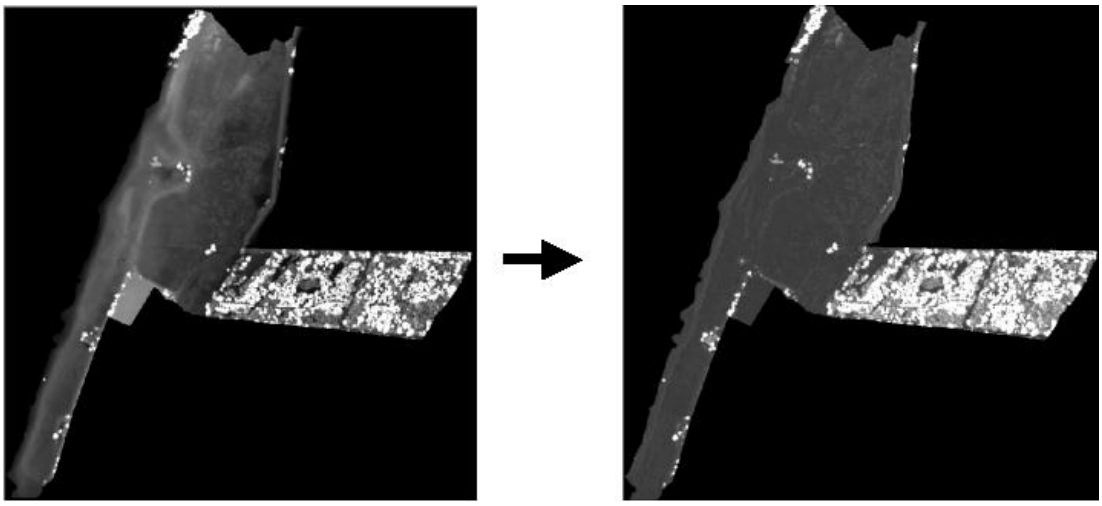

original 'MEAN' map
(vegetation + ground information)

'MEAN – DEM' map
(vegetation information only)

Fig. 14: Subtraction of the DEM

3.2.4 Change of spatial resolution

As mentioned at the beginning of this chapter, the size of the ground truth plots was approximately 3x3 meters. The pixel size of the CASI and the LiDAR (after preprocessing) images is 2x2 meters. When gathering the spectral signatures a problem of defining which pixels should be taken is found. At least one part of almost every pixel falling within a plot falls out of the ground truth area. Because of this, a decision of which pixels to take or not to take has to be done, which implies possible mistakes.

To overcome this problem, the spatial resolution of all the images was changed to 0.5x0.5 meters. In this way, each pixel was divided into 16 small pixels keeping their original value.

This procedure allowed gathering only the 'parts' of the original 2x2 meters pixels that fell inside the plots and avoided the subjective procedure of choosing which pixels must be considered for the training set.

Another advantage of changing the spatial resolution is that when the LiDAR and CASI images are stacked, the shift due to the different coordinate origin is partially avoided. In the case of stacking two images with pixel size of 2 x 2 m, the shift could be up to 1 meter. However, in our case when we stack the two images with a pixel size of half a meter, the maximum error due to a shift would be only 25 cm.

Taking into consideration the small size of our ground truth plots (3 x 3 m), this is a factor to be taken into consideration.

3.3 Image fusion

As mentioned in the introductory chapter, image fusion can take place at 3 different levels: pixel, feature and decision level.

The first approach in our research was the 'pixel level', since our first aim was to find the most straightforward method to fuse both images.

The images that were going to be fused were the ones that produced the best classification accuracy independently. Thus, the classification of the CASI and the LiDAR images separately was performed previous to deciding which images were going to be fused.

The CASI and LiDAR images that showed the best classification results were finally stacked and the classification of the fused images was carried out.

3.4 Classification

Once the problem of extracting the structural information from the LiDAR image and bringing it to the same spatial resolution as the CASI was solved, the next step was to choose a classification method. The maximum likelihood classification (MLC) and the classification tree were used for this study. The MLC is a proven and robust method which could give us a straightforward approach to classify and compare the different generated images. The classification tree analysis was chosen as an alternative to this classical classification approach. It also could add important information about the weight of each layer in the classification procedure. A brief description of these two classifiers follows this introduction about classification.

3.4.1 Maximum Likelihood Classifier (MLC)

Maximum likelihood classification is the most common supervised classification method. As a parametric classifier, the MLC algorithm relies on each training sample being represented by a Gaussian probability density function, completely described by the mean vector and variance-covariance matrix, using all available spectral bands. Given these parameters, it is possible to compute the statistical probability of

a pixel vector being a member of each spectral class (Thomas *et al.* 1987). In supervised classification, this information is derived from the training samples, which are assumed to be normally distributed within each class.

The ML classifier only calculates probabilities, so although it is used in most of the cases to analyze spectral response, other types of information can be used if the normal distribution condition is fulfilled. In our case we can make this assumption. In fact this is not the first time that MLC is used to classify texture: (Liapis *et al.* 1997; Maas, 1999). Following this criterium, the textural bands of the LiDAR image can be used with this classifier in the same way as the spectral bands of the CASI.

Although the textural bands can be input into the classifier, we have to consider that the data range of the two datasets, CASI and LiDAR, is very different. Thus, a rearrangement of the data scales had to be done before classification. All the CASI and LiDAR bands were **stretched**, using the *mean minus 2 times the standard deviation* and the *mean plus 2 times the standard deviation* as minimum and maximum values of the new scale. This is a typical stretching method which utilizes 95.44% of the values and discards the extreme minimum and maximum values (figure 15). The new scale for all the bands was the same as the CASI (16 bits, so between 0 and 65536).

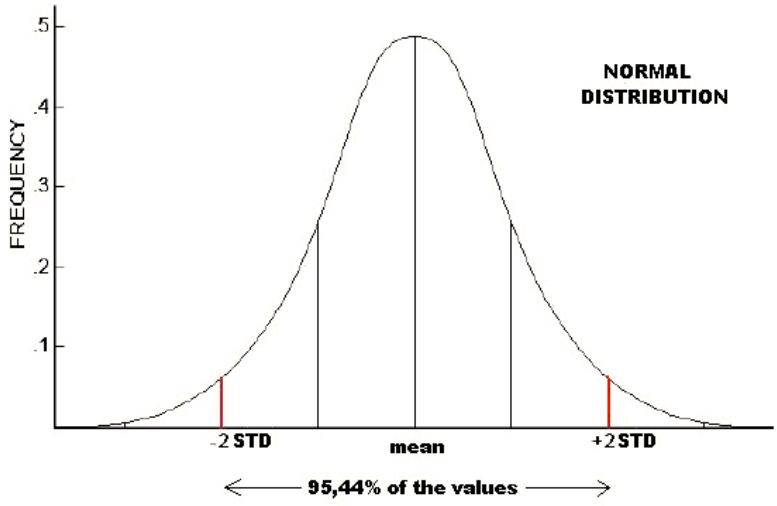

Fig. 15: Normal distribution and stretching at 2 times STD

3.4.2 Classification tree (CART analysis)

A classification tree analysis approach employs tree structured rules displayed in the form of a binary tree. The rules are determined by binary recursive partitioning in which each node of the tree is recursively split until the maximum number of nodes is reached (Cairns, 2001). Classification trees use a set of independent variables to predict class memberships. The method uses a deviance measure, the likelihood ratio statistic, to compare all possible splits of the data to find the one split that maximizes the dissimilarity among the resulting subsets (Hansen *et al.*, 1996). So, classification produces a tree through a process of *yes/no* questions generating descendent nodes. Some nodes are terminal, meaning that a final classification is reached, while other nodes continue to be split until terminal nodes are reached.

The software used to perform the classification tree analysis was CART® (Classification And Regression Trees) (Breiman *et al.*, 1984).

The CART® analysis consists of four basic steps (Lewis, 2000). The first step consists of tree building, during which a tree is built using recursive splitting of nodes. Each resulting node is assigned a predicted class, based on the distribution of classes in the learning dataset. The second step consists of stopping the tree building process. At this point a tree that fulfills the conditions derived from the learning dataset is created. The third step consists of tree "pruning," cutting off lower level splits that contribute little to the overall accuracy , which results in the creation of a sequence of simpler trees. The fourth step consists of optimal tree selection, during which the tree that fits the information in the learning dataset is selected from among the sequence of pruned trees.

The most important characteristic of this method is that for each node a threshold value is created that can be easily interpreted, which gives important information to understand the classification procedure. Moreover, the thresholds are generated without assumptions of *normality* or *continuity* of the variables, thus non-parametric and categorical variables can be included in the classification, being the best characteristic of this classification method.

The CART analysis requires the setting of the priors (probability of occurrence of each class) before starting the analysis. In this case the priors were set according to the classified fused image with the MLC. The same training data set used for MLC was used for generating the rules of the decision tree analysis. The program generated a big tree with multiple nodes (described in the results with more detail)

that was input into the *knowledge engineer* of Erdas Imagine®. In this module it is possible to input all the rules that define each terminal node of the tree and perform a classification based on such rules. In this way the classification of the final fused image (CASI + LiDAR) was performed and the classified map was obtained, so it could be compared with the result of the ML classification.

3.5 Accuracy comparisons

One of the aims of this research was to compare the classification accuracy of the CASI, LiDAR and fused images and see if there was any improvement in the classification when using both images together. The next approaches were tried to compare the different combinations before the final image was obtained by the fusion of the best results coming from the CASI and the LiDAR separately.

- From the CASI image:
1. - CASI (10 bands)
2. - PCA (1st, 2nd, 3rd and 4th principal components)

From the LiDAR image:
3. - LiDAR (search area circle 2 meters radius, min, mean, range, std, median, max)
4. - LiDAR (search area circle 4 meters radius, min, mean, range, std, median, max)

After classifying and assessing the accuracy of the first 4 images, the best result was chosen to be fused.
The layers of the CASI image and the ones of the LiDAR image were stacked together and the classification was performed for the fused image.
The images were classified with the Maximum Likelihood Classifier, following the same procedure and using the same training and accuracy assessment points, thus the randomly chosen points utilized for each procedure did not produce any bias in the final result.

Normalization of the users and overall accuracies

One of our objectives was to compare classification accuracies of different classifications. The number of ground truth points of each class used for the accuracy assessment have a direct influence on the users and overall accuracies if

the number of test points are not kept proportionally to the area of each class. For instance, one class easy to distinguish (for instance water) that has a small area in the classified image would bias the users and overall accuracies if the number of test points were not proportional among the different classes. Just increasing the number of test points in that class would increase the overall accuracy and users accuracy of that class, which would make no sense. Hence, the number of testing points for each class should be proportional to the area of each particular class, as shown in figure 16.

However, in most of the cases we do not know the area of each class before starting the analysis. In this case, a good approach would be to rearrange the number of test points in the error matrix according to the area that each class has in the classified image. This procedure is also not error-free because the normalization of the error matrix would come from areas of the classified image, which indeed is not perfect. However, it is better than not taking this factor into consideration at all.

So in this way, all the *users* and *overall* accuracies were normalized according to the number of test points available for each class and their respective area in the classified image.

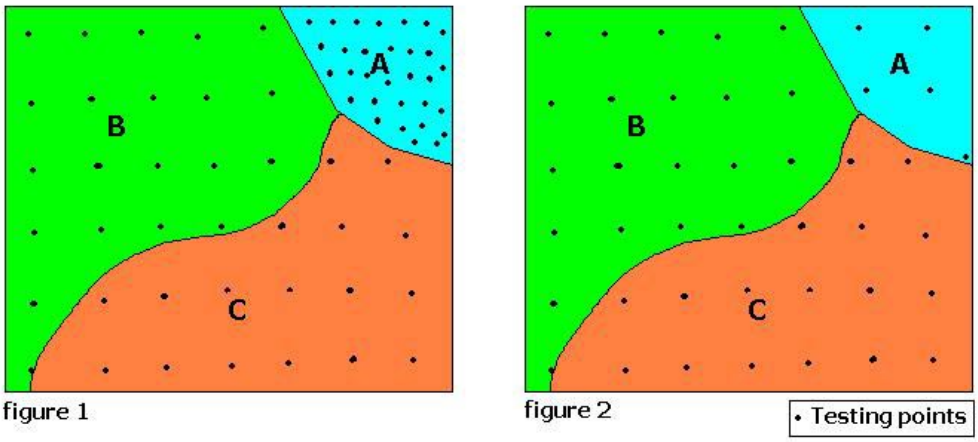

Fig. 16: The number of testing points should be kept proportional to the area of each class. In the figure 1, the class A is overestimated and would affect the overall and the users accuracy of that class. The figure 2 shows the ideal testing points sampling scheme. This ideal situation is approached (a posteriori) by the normalization of the error matrices.

4 Results and discussion

4.1 Rastering of the LiDAR data

As described in section 3.2.2 regular grids of 2x2 m were created from the LiDAR data. Grid cell values consisted of height statistics (section 3.2.2.2) derived by considering different search areas around the cell center (figure 10)

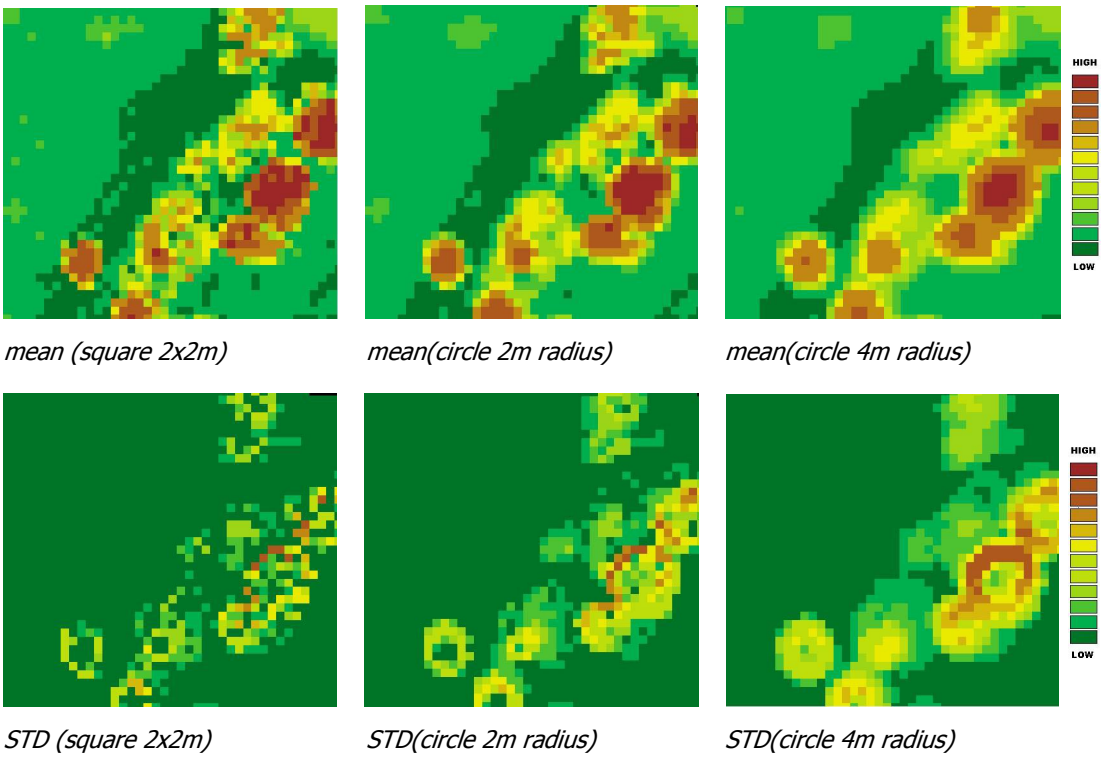

mean (square 2x2m) *mean(circle 2m radius)* *mean(circle 4m radius)*

STD (square 2x2m) *STD(circle 2m radius)* *STD(circle 4m radius)*

Fig. 17: Comparison between different 'search areas' for the LiDAR image

Figure 17 represents different LiDAR images of the same area: a small, partially forested part of the study area of about 80 x 80 meters. The features that are delineated correspond to trees. The image with a square search area of 2x2 meters produced a scattered result compared to the other two, where the features are more distinguishable. Another aspect to point out is that the bigger the search area, the smoother is the result, but also part of the detail is lost. It is easy to reason that increasing the search area too much would produce a very smooth image, from which no information could be extracted. What is important is the local variation of height; so in theory, the smaller the search area the more accurate the result. However, this hypothesis would be correct only if the density of LiDAR points was

very high. In our case, one point per square meter was not enough to derive reliable statistics in small search areas. That is why the map coming from a search area of 2 x 2 meters shows poor results in this study. On the other hand, the problem of using larger search areas (in order to have more points to derive statistics) is that the calculations would come from height values which lay very far from the pixel we are trying to assign a texture value to, which introduces an error of assumption. Moreover, also the scale of the study should be taken into consideration when we choose the size of the output pixel and the search area.

Another important aspect is the different range of texture values that the different classes show. The texture values of the class 8 (*forest*) are much higher than those in the rest of the classes, in the order of 50 to 100 times bigger. This means that for the whole image, when scaled between the minimum and the maximum, the result is an almost complete visual homogenization of the classes from 1 to 7 (because of their low texture values compared to the class *forest*). This fact gives the impression of a lack of ability of the LiDAR image to discriminate features between the low vegetation classes. However, rescaling the texture values within the low vegetation classes will show that even small differences in vegetation height are visible (and thus analyzable) in the LiDAR composite. This can be seen in figure 18.

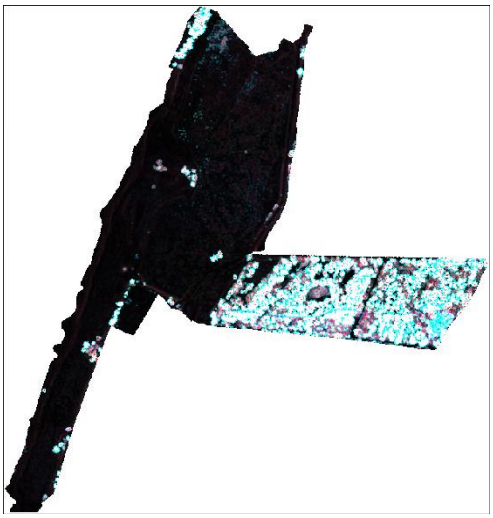

composite range, std, mean (R G B)
original image

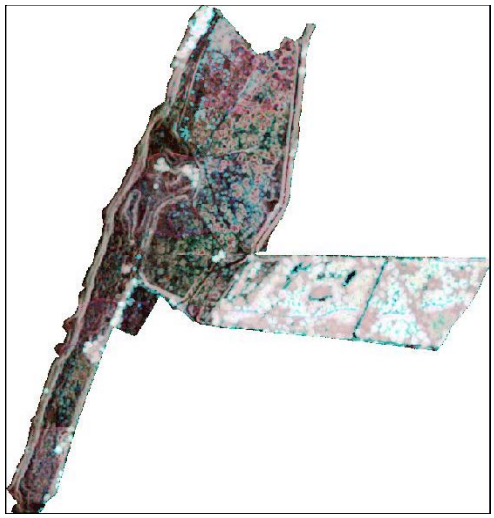

composite range, std, mean (R G B)
after histogram equalization

Fig. 18: Visualization of the 'hidden' information of the LiDAR image

4.2 LiDAR ML classification results

As mentioned in the methodology, the Maximum Likelihood Classifier was used to classify the LiDAR images. A total of 170 ground truth plots were used as training data-set and 164 as testing. The plots were selected randomly. As stated before, the LiDAR images with **circular search areas** of **2** and **4 meters radius** were used for further analysis.

The result of the classification is shown in table 3.

	LiDAR 2m radius		**LiDAR 4m radius**	
	Users accuracy normalized	Producers accuracy	Users accuracy normalized	Producers accuracy
Class 1	31.78%	54.55%	26.64%	72.73%
Class 2	13.31%	57.89%	0.00%	0.00%
Class 3	7.23%	11.54%	10.63%	15.38%
Class 4	22.82%	23.26%	22.89%	39.53%
Class 5	9.52%	5.26%	23.88%	15.79%
Class 6	0.00%	0.00%	84.76%	13.64%
Class 7	6.78%	50.00%	44.94%	100.00%
Class 8	100.00%	90.00%	99.07%	100.00%

	LiDAR 2m radius	**LiDAR 4m radius**
Overall accuracy	**30.67%**	**35.58%**
Overall normalized accuracy	**33.68%**	**43.36%**

Table 3: Classification accuracy comparison between LiDAR 2m and LiDAR4m

The LiDAR image coming from a circular search area of 4 meters radius (LiDAR 4m_radius) showed the best overall accuracy. Also the producers and users accuracy was better in almost all the classes, especially in classes 7 and 8, which are the ones with the clearest structural pattern. According to this result, this image was chosen to be fused with the CASI image.

The most important remark about the results of the classification of the LiDAR image is that LiDAR was able to classify the classes 7 and 8 quite well. The rest of the classes appeared rather mixed, including the class 1 (sandy bare soil).

The problems of the LiDAR image to classify the class number one comes from the low accuracy of the DEM and the slope of the terrain in that class. When a DEM, which comes from an initial resolution of 6 x 6 meters is subtracted from the 2x2 m pixels height values of the LiDAR image, the result in steep zones is a 'stepwise' pattern perpendicular to the slope, which makes confusion with height values coming from vegetation. Moreover, large search areas in steep zones produce also values of relative height that can be confused with differences of vegetation height. This problem would be solved with a more accurate DEM or with a higher LiDAR point density, which would allow smaller search areas.

The LiDAR was not able to discriminate properly the rest of the classes, from 2 to 6, most probably because those classes do not show evident differences in their structure.

As a final remark we can say that the size of the search area showed a clear influence on the result of the classification.

4.3 CASI ML classification results

The CASI image was classified using the same ground truth points and testing points for the classification accuracy. Figure 19 shows the spectral signature of the 8 classes in the CASI image. We can see that the spectral signatures of class 1 and 8 are clearly distinct to the rest, whereas the rest (from 2 to 7) appear rather overlapped. This was reflected in the classification results.

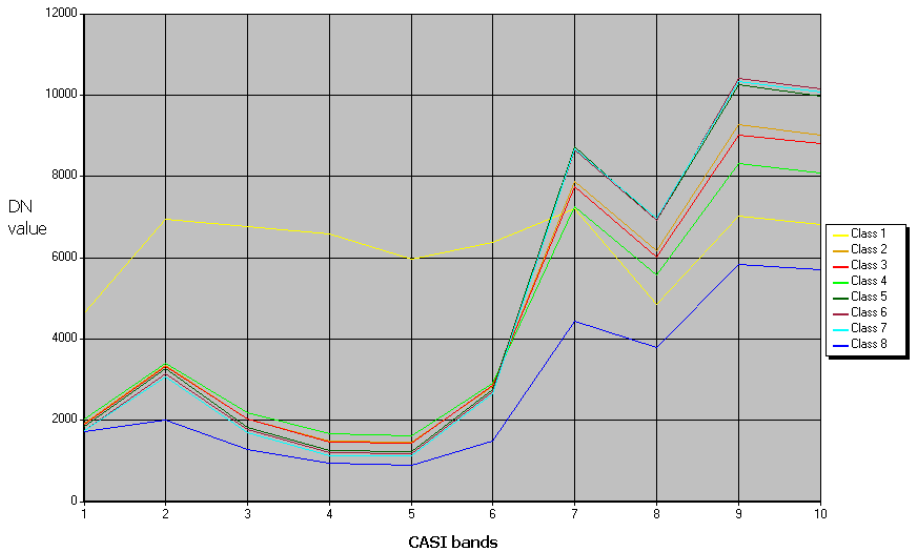

Fig. 19: Spectral signatures of CASI

The PCA was also performed and the obtained image (section 3.2.1.1) was classified. In this case also class 1 and 8 appear clearly distinct whereas de rest are quite mixed (figure 20).

The results were compared to those of the CASI. We can see the results in the accuracy reports in table 4.

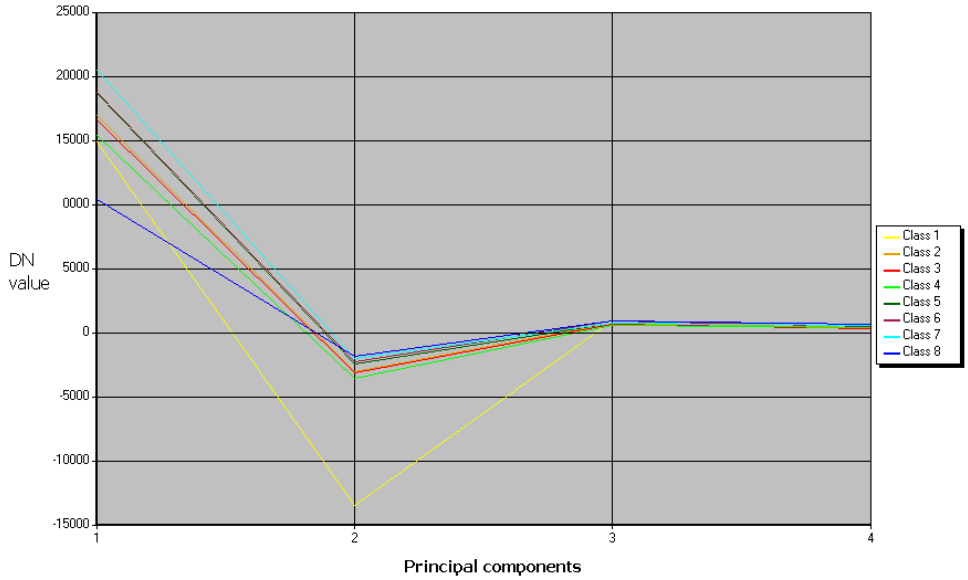

Fig. 20: Spectral signatures of PCA

	CASI		PCA	
	Users accuracy normalized	Producers accuracy	Users accuracy normalized	Producers accuracy
Class 1	86.9%	100.00%	91.67%	100.00%
Class 2	33.6%	31.58%	21.43%	15.79%
Class 3	58.58%	42.31%	28.57%	23.08%
Class 4	41.0%	46.51%	68.75%	51.16%
Class 5	49.4%	68.42%	57.14%	42.11%
Class 6	52.7%	54.55%	30.95%	59.09%
Class 7	24.9%	33.33%	0.00%	0.00%
Class 8	97.3%	95.00%	100.00%	100.00%

	CASI	PCA
Overall accuracy	**57.06%**	**51.23%**
Overall normalized accuracy	**55.60%**	**53.46%**

Table 4: Classification accuracy comparison between the original CASI bands and the first 4 principal components (PCA)

Neither CASI nor PCA were able to clearly discriminate classes from 2 to 7. Moreover, the PCA did not show any improvement of the classification. Thus, according to the classification results, the original CASI image was chosen to be fused with the LiDAR.

4.4 ML classification results after fusion of CASI and LiDAR data

Once the LiDAR image was transformed into a regular grid with textural information, the different layers coming from the LiDAR were stacked together with those from the CASI, creating a new image containing all the bands.

The result of this fusion can be better understood in the figure 21, where we can see a composite image made from two bands of the CASI (blue and green) and the band *max* of the LiDAR (red). Zooming into the image, we can even appreciate how the trees are enhanced by the LiDAR band (*max*), whereas the shadows of the trees are delineated by the CASI bands.

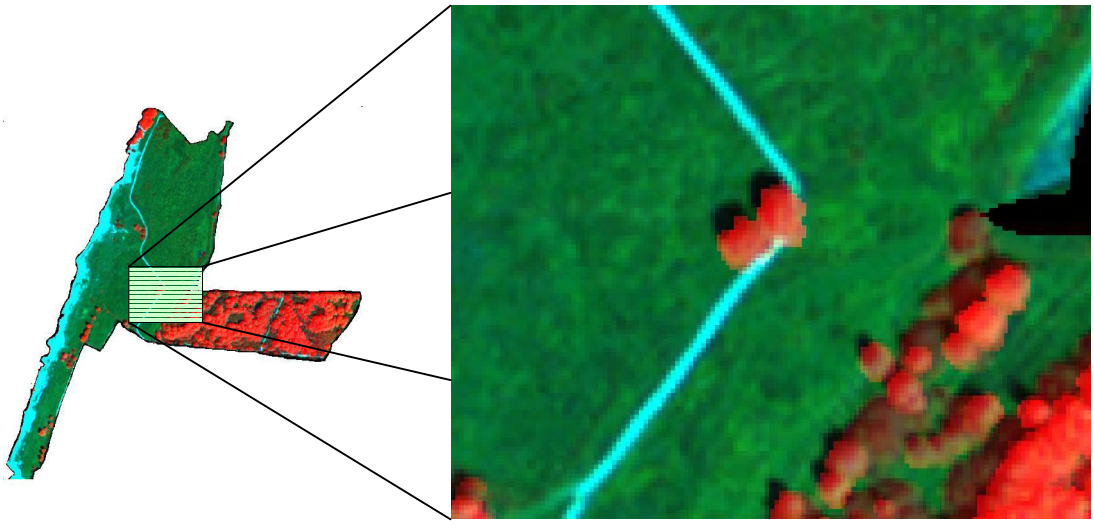

Fig. 21: Fused image of CASI + LiDAR. Composite RGB (*max*, green, blue)

This is just an example to show that the information of CASI and LiDAR was integrated into the same image and therefore can be visualized and analysed simultaneously.

All the CASI and LiDAR bands were stretched (section 3.4.1) and the image was classified using the same ground truth points and the results compared to those coming from the CASI and the LiDAR alone.
In table 5, the overall accuracies of the different classifications are shown, including the two of the LiDAR, CASI and PCA described already before.

Image	*Overall accuracy*	*Overall normalized accuracy*
LiDAR 2m_circle	***30.67%***	***33.68%***
LiDAR 4m_circle	***35.58%***	***43.36%***
CASI (10 bands)	***57.06%***	***55.60%***
PCA (1 – 4 principal component)	***51.23%***	***53.46%***
FUSED (CASI + (LiDAR 4m_circle)	***56.44%***	***63.52%***

Table 5: Overall accuracies of the different classifications.

Looking at the overall accuracy, the classification results of the fused image is almost the same as those of the CASI data. On the other hand, the normalized overall accuracies showed an improvement for the fused image (table 8). However, these values have to be studied more carefully before drawing definite conclusions.
An analysis of the error matrix is needed to see the influence of the fusion of the two images on the final results. At this point it must be said that the large number of layers used for the analysis, the redundancy and/or contradiction that some layers could add at the classification process, might have an influence on the final classification, which cannot be analyzed with this classification method. Is the ML classifier able to leave aside the information of 'noisy layers' and use only the important ones? This is one of the drawbacks of the ML classifications. There is no *a posteriori* information that could help us to understand the influence of each layer better during the classification procedure.
Despite that problem, we can draw some important conclusions from the error matrices (appendixes D to H).
- Class 1 is well classified in all the images, except for the LiDAR alone. In this case the most important characteristic of this class is the complete unique spectral response, which makes it easily classified by the CASI image. The spectral signature of each class can be seen also in figure 19.

- Class 8 (forest) is perfectly classified by the LiDAR, fused and PCA images. In this case not only the spectral response, but also the structure is unique of this class.
- The rest of the classes are often misclassified. They all show a similar spectral response and also have a not very distinguishable physical structure. However, there is an important observation to be made.

LiDAR and the fused images classify class 7 better, which has a distinct structure but not a distinct spectral response, whereas the CASI and the derived PCA images are not that effective to discriminate this class.

Another important remark is that although we cannot find out the weight of each image (CASI and LiDAR) in the ML classification procedure, it is clear from the analysis of the error matrix (appendix E) that the fusion of the two images produced an homogenization of the classification. This means that the distribution of the wrongly classified plots among the other classes is more homogeneous in the fused image. Taking into consideration that we are talking about structural classes ordered by height (from 1, the lowest, to 8, the highest), the homogenization can be considered as an improvement.

For example, let's assume that one plot belonging to class 7 is classified as class 2 in the CASI image, but as class 6 in the fused image. According to the overall accuracies, both classifications are mistaken, but considering that class 7 is more 'similar' to class 6 than to class 2 (see figure 8), we could conclude that the fused image classified 'better' (or at least less wrongly) than the CASI in that case. This effect can be appreciated in the next *schematic* error matrices (figure 20). Green represents correct classifications, red wrong classifications and light blue 'not misclassified'. To make it clearer, let's say that a perfectly classified image would be represented by a green diagonal with only blue cells in the rest of the table. In this scheme, the values are not shown, it is only an idea of the 'homogenization' of the classification.

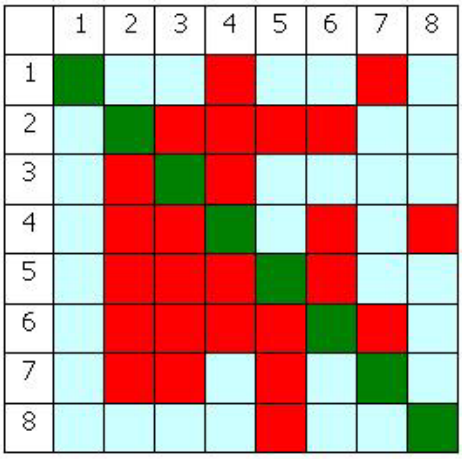

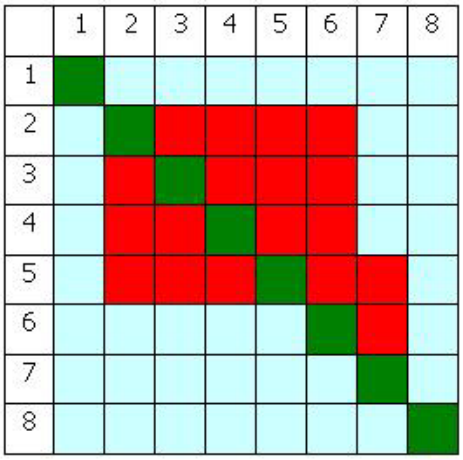

CASI **FUSED (CASI + LiDAR)**

Fig. 22: Schematic error matrices. Values are not shown, only the concept of *homogenization*, which is shown by the distance of the mistakes to the central diagonal. The *homogenization* of the mistakes is better in the FUSED images

Summarizing, the fusion of the two images produced an improvement of the overall accuracy (from **55.60%** to **63.52%**). This improvement has to be analyzed carefully, because we could see that the non-proportional distribution of the testing points in the sampling scheme had a strong influence on the final results.

However, the effect of the LiDAR was clear in the fused image, producing, as explained before, a more homogeneous classification of the different structural vegetation classes, closer to our aim. This means that the structural information added by the LiDAR image was effectively used by the ML classifier and helped to discriminate the different structural classes.

4.5 Results of Decision Tree classification

As mentioned in the methodology chapter, a different approach used to analyze the fused image was the *decision tree classification* (CART analysis). The results are similar to those of the ML classifier, and show the existing spectral and structural mix of the classes from 2 to 6, while on the contrary the producers and users accuracy of the classes 1 and 8 are 100% (table 8).

One important aspect of this classification method is that the program generates its own classification thresholds for each class combining information from different bands. The range value of the bands does not need to be normalized or rescaled. Moreover, after the classification, a rank of importance of each band for the

classification procedure is given, which can be very valuable to understand the weight of each layer during the classification procedure. This information is missing with the ML classifier.

Another option to gain extra information about the variable importance is analyzing the structure of the tree visually, which can help to understand better the classification process (figure 23). We can see which variables play a role in the first splits, normally the most important ones. In our case, the final tree presented 315 terminal nodes. Each one of these nodes is a decision rule for a fixed class, determined by a combination of threshold values of different layers. Taking a look at our tree, we can draw some conclusions.

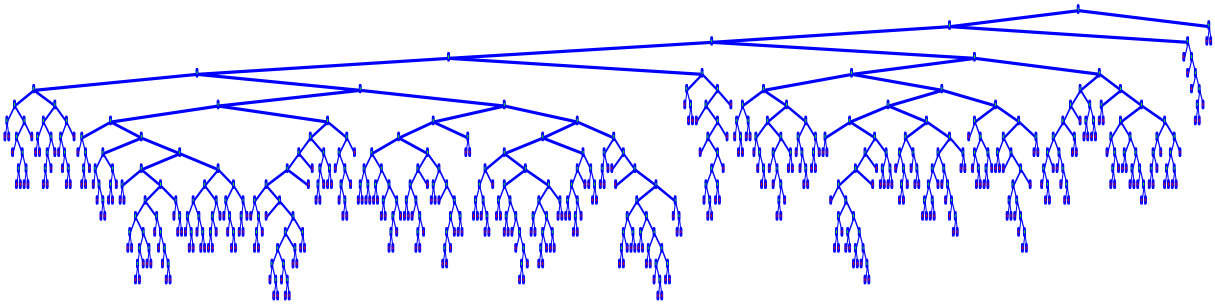

Fig. 23: Structure of the decision tree generated by CART

The classes 1 and 8 were defined with only a few nodes, whereas the rest of the classes were classified with multiple nodes, sometimes differentiated by very narrow threshold values. This fact confirms the already mentioned problem of the mixing of classes from the class 2 to 7. While the CART analysis can identify classes 1 and 8 with a few nodes, it cannot do the same with the rest of the classes and has to create multiple nodes to generate the rules for discriminating the rest of the classes, which ends up creating a huge and confusing tree which is not able to classify properly the mixed classes. In table 6, the number of terminal nodes generated by CART to define each class is shown. It is derived from the tree shown in figure 23.

Class	*Class 1*	*Class 2*	*Class 3*	*Class 4*	*Class 5*	*Class 6*	*Class 7*	*Class 8*
Number terminal nodes	*4*	*54*	*74*	*71*	*45*	*55*	*10*	*2*

Table 6: Classification tree: Number of terminal nodes generated per class

As mentioned in the methodology, another important characteristic of the decision tree analysis is the possibility of analyzing the weight of each layer in the classification. Table 7 was generated by the CART analysis, and shows the variable importance ranking during the generation of the tree.

Variable	*Score*	
C6	*100.00*	//
LMAX_16	*85.11*	//////////////////////////////////////
LSTD_13	*84.52*	//////////////////////////////////////
LRANG_12	*84.44*	//////////////////////////////////////
LMEAN_15	*82.69*	//////////////////////////////////////
LMED_14	*77.73*	//////////////////////////////////
C4	*53.82*	////////////////////////
C5	*53.51*	////////////////////////
C1	*44.04*	//////////////////
C3	*42.21*	//////////////////
C2	*40.57*	//////////////////
C9	*26.35*	//////////
C10	*25.58*	//////////
C7	*21.83*	////////
C8	*21.56*	////////
LMIN_11	*3.16*	

Table 7: Variable importance of each band

However, the analysis of the variable importance ranking of the CART analysis is very complicated because it comes from this specific tree and because the way it is generated and interpreted is not clear. Other trees with similar accuracies could have been generated and could have produced different variable importance rankings.

Hence, despite these conclusions, the use of CART analysis requires a thorough study and this test was only a first approach to this promising classification methodology. The possibilities that the CART analysis can offer in the field of the fusion of CASI and LiDAR are open for further studies.

In table 8 the accuracy reports of the fused images classified with *decision tree analysis* and Maximum Likelihood are compared.

	Maximum Likelihood		Decision tree (CART analysis)	
	Users accuracy Normalized	Producers accuracy	Users accuracy normalized	Producers accuracy
Class 1	100.00%	100.00%	100.00%	100.00%
Class 2	22.55%	21.05%	30.85%	36.84%
Class 3	39.90%	61.54%	22.62%	26.92%
Class 4	46.41%	53.49%	38.74%	67.44%
Class 5	48.31%	63.16%	35.56%	26.32%
Class 6	91.26%	22.73%	25.27%	13.64%
Class 7	100.00%	66.67%	45.07%	33.33%
Class 8	100.00%	100.00%	100.00%	100.00%

	Maximum Likelihood	Decision tree (CART analysis)
Overall accuracy	**56.44%**	**50.92%**
Overall normalized accuracy	**63.52%**	**53.65%**

Table 8: Classification accuracies comparison between MLC and decision tree analysis for the fused image.

5 Conclusions and Recommendations

5.1 Conclusions

After the results have been obtained and discussed, it is time to look back and draw conclusions about this study. The main objective of this thesis was to perform a vegetation classification (according to structural classes) combining CASI and LiDAR images. This objective was fulfilled. A classification of the vegetation in the floodplain of the river Rhine in The Netherlands, using the CASI and the LiDAR datasets together was done. To achieve this, first a methodology to extract information from the LiDAR image was successfully developed. The grid maps coming from statistical calculations of LiDAR height points were useful to discriminate different structural classes. The use of the original LiDAR points for deriving the statistical calculations and generate the grid maps was an improvement, compared to other methods. Moreover, trying different search areas to extract information showed that this is an important factor to take into consideration when analyzing the LiDAR dataset.

The fusion of the CASI and LiDAR datasets was possible by means of the rasterization of the LiDAR image. The classification of the fused image showed an improvement, not only on overall accuracy but also on homogenization of the errors, compared to the classification based on spectral information only (from **55.60%** to **63.52%**). This fact supported the hypothesis that the LiDAR image would help in classifying structural patterns. Moreover, the ML classifier was able to use in an effective way the information coming from the two datasets.

However, the results of the classification revealed a problem of definition of the different structural classes. The merging of ecological communities into structural classes failed to some extent, since none of the approaches was able to clearly discriminate from class 2 to 6. The inclusion of the LiDAR only made possible to improve the classification of class 7, which has a fairly distinguishable structural pattern. The conclusion about this failure is that classes from 2 to 6 had similar structural and spectral pattern and so were not classified correctly. So we would not say that the CASI and LiDAR were not capable to classify properly, but quite the opposite they were able to show evidences about the overlapping of those classes.

About the use of a different classification approach, the decision tree classification, we can conclude that the results were worse than those of the ML classifier. On the other hand, the classification was useful to confirm the same class mixing problem and, moreover, important information about the different layers of CASI and LiDAR was generated. However, the complexity of the CART outputs did not permit a thorough analysis of all the possibilities that this classification method offers and so, the use of decision tree analysis for analyzing LiDAR and CASI data remains open for further analysis.

5.2 Recommendations

During the development of this research we faced and solved many problems. The experience acquired allows us to give some recommendations that can be used for further studies concerning the fusion of multispectral and laser scanning data or other similar studies.

The design of the **sampling scheme** should always be based on the purpose of the study. Basing the definition of our classes on a previous study that had not as purpose the analyzing of structural classes, yielded a problem in that the information did not match our needs. In our case, more homogeneous classes and also bigger sampling areas would have improved the final classification.

Since we were trying to classify vegetation, the use of **multitemporal data** could also help to discriminate between classes that could show differences in a certain time of the year.

Regrouping of the structural classes into 4 is recommended. The four classes could be merged as follows: bare soil or grass, low-medium vegetation, medium-high vegetation (bushes) and forest. These four classes could be reasonably well classified with the available datasets and could be of help for the river manager.

Concerning the **LiDAR**, several aspects could improve the quantity and quality of the information that this data sources can offer.

If possible, **increasing the point density** of the LiDAR image can help to use smaller search areas and consequently yield a higher accuracy and more reliable statistics.

The use of **different search areas** for each the statistical parameter could also improve the extraction of information from the LiDAR image.
Search areas should have the size of the output pixel only if there are enough points to derive reliable statistics.
The **better understanding** of the characteristics of the **vegetation classe**s under study can help to chose the right statistical parameters to analyze and even avoid the redundancy given by correlated parameters.
For vegetation studies like this one, the use of the **first and last pulse** simultaneously is crucial and can give very valuable information, allowing taking decisions almost at point level. The possibility of generating a very reliable DTM, avoiding any influence of the relieve and focusing only on vegetation can produce significant improvements.
The use of **spatial statistical techniques**, like variogram analysis at pixel level can increase the amount of information extracted from the LiDAR image. Some patterns that are not seen with simple statistical parameters can become clear with a thorough spatial statistical analysis.

Concerning the fusion phase, although the method developed in this study was the most straightforward possible, other approaches are also valid. As explained in chapter 2.4.3, **feature level classification**, using the LiDAR and CASI separately, to differentiate different classes step by step can be a good approach. We could take advantage of the special capabilities of each data set without interference of the others during the classification.

6 References

Ackermann F. (1999). **Airborne laser scanning - present status and future expectations**. ISPRS Journal of Photogrammetry & Remote Sensing, 54(2-3): 64-67.

Alharthy A., J. Bethel (2002). **Heuristic filtering and 3D feature extraction from LiDAR data.** Proceedings of the ISPRS Technical Commission III Symposium 2002. September 9 – 13, 2002, Graz, Austria.
http://www.isprs.org/commission3/proceedings/papers/paper061.pdf

Asselman, N. (2001). **Laser altimetry and hydraulic roughness of vegetation**. WL Report Q2701. Delft: WL, Delft Hydraulics.

Axelsson, P. (1999). **Processing of laser scanner data algorithms and applications**. ISPRS Journal of Photogrammetry & Remote Sensing, 54, pp 138-147

Baltsavias, E. P. (1999). **Airborne laser scanning: existing systems and firms and other resources**. ISPRS Journal of Photogrammetry and Remote Sensing, 54, (N2-3): 164-198

Blair, J. B., D. L. Rabine, M. A. Hofton (1999). **The Laser Vegetation Imaging Sensor: a medium-altitude digitasion-only, airborne laser altimeter for mapping vegetation and topography**. ISPRS Journal of Photogrammetry and Remote Sensing, 54, 115-122.

Breiman L., J.H. Friedman, R.A. Olsen, C. J. Stone (1984). **Classification and Regression Trees**. Wadsworth, Belmont.

Cairns, D. M. (2001). **A comparison of methods for predicting vegetation type**. Plant Ecology 156: 3-18

Chica-Olmo, M. and F. Abarca-Hernandez (2000). **Computing geostatistical image texture for remotely sensed data classification**. Computers & Geosciences v. 26, no.4, pp. 373-383.

Cobby, D.M., D.C. Mason, and I.J. Davenport (2001). **Image processing of airborne scanning laser altimetry for improved river flood modelling**. ISPRS J. Photogrammetry & Remote Sensing, 56, 121-138

Flood, M., and B. Gutelius. (1997). **Commercial implications of topographic terrain mapping using scanning airborne laser radar**. Photogrammetric Engineering and Remote Sensing, 63, 327-329, 363-366.

Gong P., R. Pu, and J.R. Miller (1995). **Coniferous Forest Leaf Area Index Estimation along the Oregon Transect using Compact Airborne Spectrographic Imager Data**. Photogrammetric Engineering And Remote Sensing, Vol. 61:9, pp. 1107-17.

Haack, B. and M. Bechdol (2000). **Integrating multisensor data and RADAR texture measures for land cover mapping**. Computers & Geosciences, Vol 26, No 4, May. pp. 411-421

Hahn M., E. Baltsavias (1998). **Cooperative algorithms and techniques of image analysis and GIS**. International Archives of Photogrammetry and Remote Sensing. Volume XXXII, Part 4
http://www.ifp.uni-stuttgart.de/publications/commIV/hahn13neu.pdf

Hansen, M., R. Dubayah and R. Defries (1996). **Classification trees: an alternative to traditional land cover classifiers**. International Journal of Remote Sensing. Vol 17 No 5: 1075-1081.

Hill R. A., G. S. Smith, R. M. Fuller, and N. Veitch (2002). **Landscape modelling using airborne multi-spectral and laser scanning data**. International Journal of Remote Sensing. Vol 23, No 11, 2327-2334.

Irish, J. L., J. K. McClung and W. J. Lillycrop (2000). **Airborne lidar bathymetry: the SHOALS system**. PIANC Bulletin, No. 103–2000, 43-53

Kurnatowska, A. M. (1998). **Large-scale vegetation mapping in mountain environments using remote sensing and plant physiology methods**. Operational Remote Sensing for Sustainable Development, G.J.A., Nieuwenhuis, R.A., Vaughan and M. Molenaar (Eds.), Balkema, Lisse, pp. 61-65.

Lefsky M. A, W. B. Cohen, S. A. Acker, G.G. Parker, H.H. Shugart (1999). **LIDAR remote sensing of the canopy structure and biophysical properties of Douglas-Fir Western Hemlock Forests**. Remote Sensing of the Environment 70:339-361

Lefsky M. A., W. B. Cohen, G. G. Parker, D. J. Harding (2002). **Lidar remote sensing for Ecosystem Studies**. BioScience, Vol. 52 No.1

Lewis, R. J. (2000). **An Introduction to Classification and Regression Tree (CART) Analysis**. San Francisco, California., Department of Emergency Medicine Harbor-UCLA Medical Center Torrance**:** 1-14.

Liapis S., N. Alvertos and G. Tziritas (1997). **Maximum likelihood texture classification and Bayesian texture segmentation using discrete wavelet frames**. International Conference on Digital Signal Processing, Santorini.
www.csd.uch.gr/~tziritas/papers/texture.pdf

Lillesand T. M. and R. W. Kiefer (2000). **Remote Sensing and Image Interpretation, Fourth Edition**: John Wiley and Sons Inc. New York, 724 p.

Mass, G-H. (1999). **The potential of height texture measures for the segmentation of airborne laser scanner data**. Presented at the 4th Airborne Remote Sensing Conference and Exhibition Ottawa, Ontario, Canada. 21-24th June 1999

Means, J. E., S. A. Acker, D. J. Harding, J. B. Blair, M. A. Lefsky, W. B. Cohen, M. E. Harmon, and W. A. McKee (1999). **Use of large-footprint scanning airborne lidar to estimate forest stand characteristics in the Western Cascades of Oregon**. Remote Sensing of Environment, 67, 298-308.

Miranda, F., L. Fonseca and J. R. Carr (1998). **Semivariogram textural classification of JERS-1 (Fayo-1) SAR data obtained over a flooded area of the Amazon rainforest**. International Journal of Remote Sensing, Vol. 19, No. 3

Muhammad, S. (2002). **Extraction of Urban and Rural Features by Using Image fusion Techniques and Neural Networks**. Centre for Geoinformation. Wageningen, Wageningen University: 80 pp.

Naesset, E. (1997). **Estimating timber volume of forest stands using airborne laser scanner data**. Remote sensing of the environment, 61 p. 246-53.

Nilsson, M. (1996). **Estimation of tree heights and stand volume using an airborne lidar system**. Remote Sensing and Environment 56: 1-7

Pohl, C., and J. L. van Genderen (1998). **Multisensor image fusion in remote sensing: concepts, methods and applications**. International Journal of Remote Sensing, 19(5): 823-854.

Protz R., A. J. Van den Bygaart, M. D. Wood and B. G. A. Hulshof (1999). **Evaluation of High Resolution Airborne Imagery and Global Positioning Systems for Monitoring Changes in Agro ecosystems**. COESA, Report No.: RES/MON-012/97

RIZA (1999). **Twice a river: Rhine and Meuse in the Netherlands**. Ministry of Transport, Public Works and Water Management. Directorate-General for Public Works and Water Management. Riza Institute for Inland Water Management and Waste Water Treatment.

Shang, J., M. Y. Jollineau, P. J. Howarth and J. Wang, (1998). **A comparison of spatial- and spectral-mode CASI imagery for coastal wetland mapping in the Lake St. Clair delta: preliminary results**. Proceedings of the 20th Canadian Symposium on Remote Sensing, Calgary, Alberta, May 1998, pp. 215-218

Shang, J. J. Levesque, P. Howarth, W. Morris, K. Staenz and P. Yearwood, (1999). **Preliminary investigation of acid mine drainage detection using CASI data.**

Copper Cliff, Ontario, Canada. Proceedings of the 4th International Airborne Remote sensing Conference and Exhibition / 21st Canadian Symposium on Remote Sensing, Ottawa, Ontario, June 1999, Vol. I, pp. 771-778

Skidmore, A. K., C. Varekamp, L. Wilson, E. Knowles, and J. Delaney (1997). **Remote Sensing of Soils in a Eucalypt Forest Environment**. International Journal of Remote Sensing, Vol 18:1 pp.39-56

Smith R. A., J. L. Irish, M. Q. Smith (2000). **Airborne LiDAR and Airborne Hyperspectral imagery: A fusion of two proven sensors for improved hydrographic surveying**. Proceedings, Canadian Hydrographic Conference 2000, Montreal, Canada. http://shoals.sam.usace.army.mil/pdf/Smith_Irish_Smith_00.pdf

Song, Jeong-Heon, Soo-Hee Han, Kiyun Yu,Yong-Il Kim (2002) **Assessing the possibility of land-cover classification using LiDAR intensity data.** Proceedings of the ISPRS Technical Commission III Symposium 2002. September 9 – 13, 2002, Graz, Austria.
http://www.isprs.org/commission3/proceedings/papers/paper128.pdf

Thomas, I., V. Benning, N. Ching (1987). **Classification of Remotely-Sensed Images** (Bristol: IOP).

Von Hansen, W., M. Sties (2000). **On the capabilities of digital high resolution multispectral remote sensing techniques to serve nature conservation requirements**. International Archives of Photogrammetry and Remote Sensing, Vol. XXXIII, Part B7.

Wehr, A. and U. Lohr (1999). **Airborne laser scanning – an introduction and overview**. ISPRS Journal of Photogrammetry and Remote Sensing, 54 (2-3): 68-82.

7 Appendixes

Appendix A: Classified images LiDAR 2m and LiDAR 4m

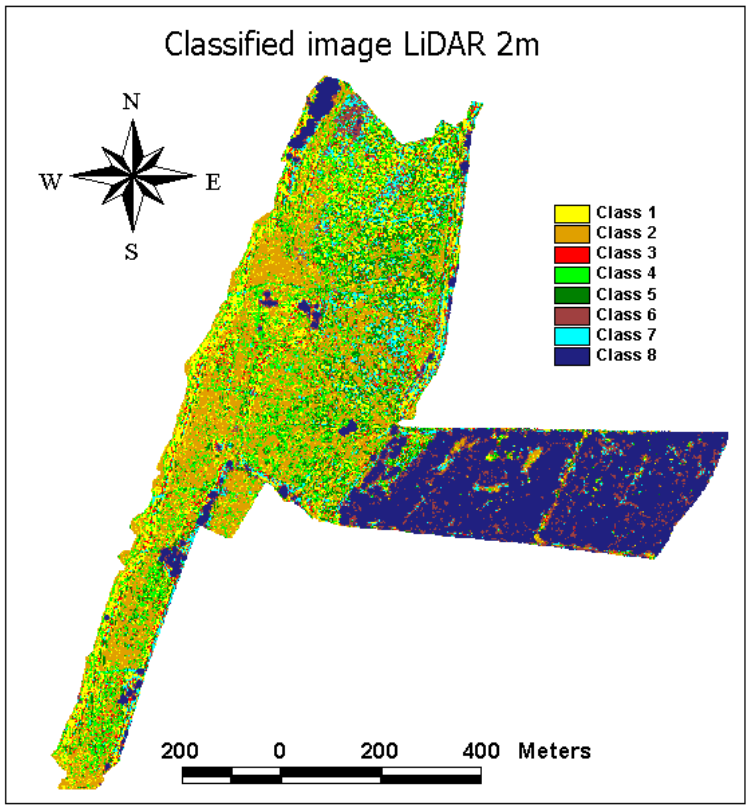

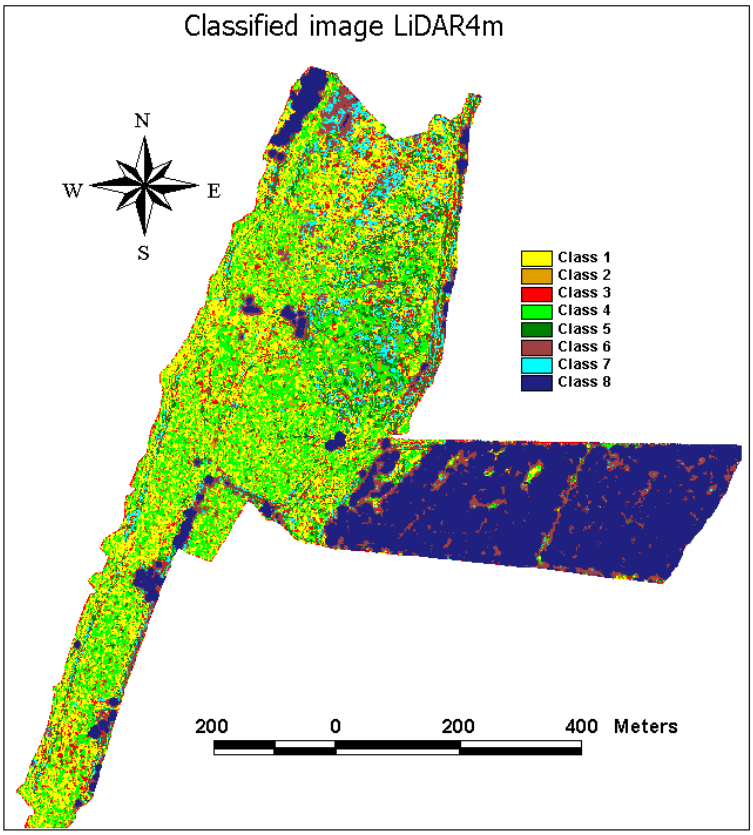

Appendix B: Classified images CASI and PCA

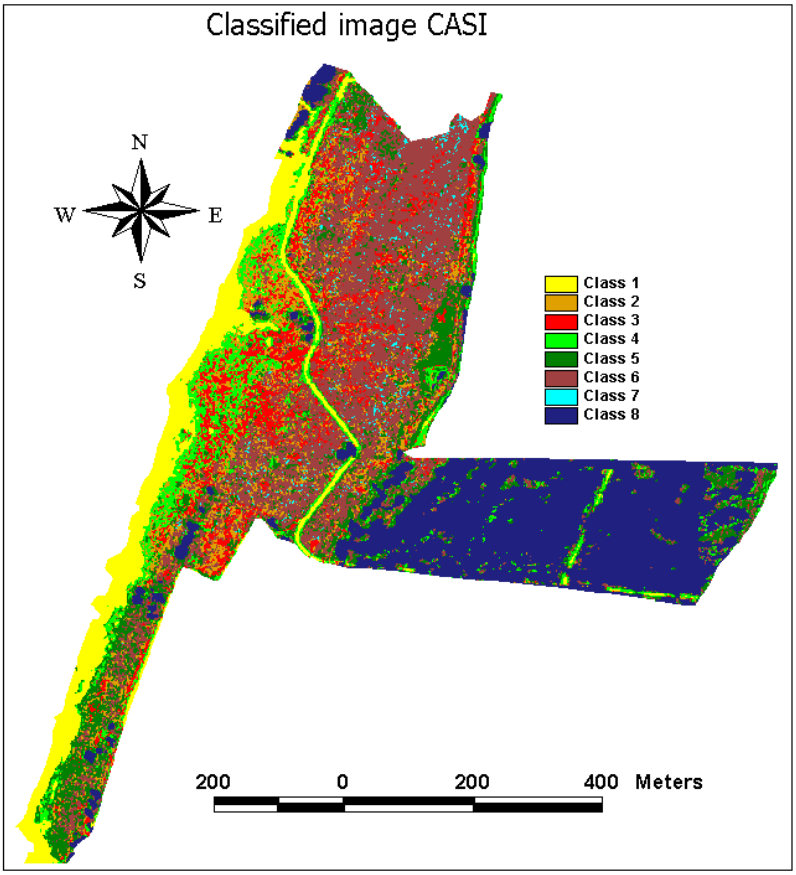

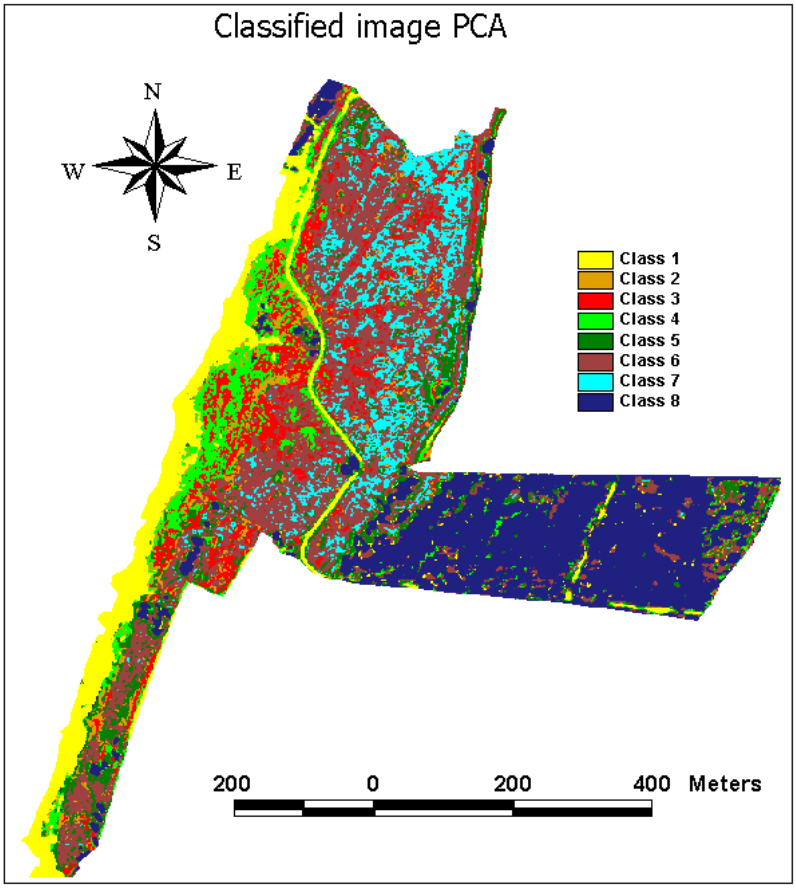

Appendix C: Classified images Fused MLC and Fused Decision Tree

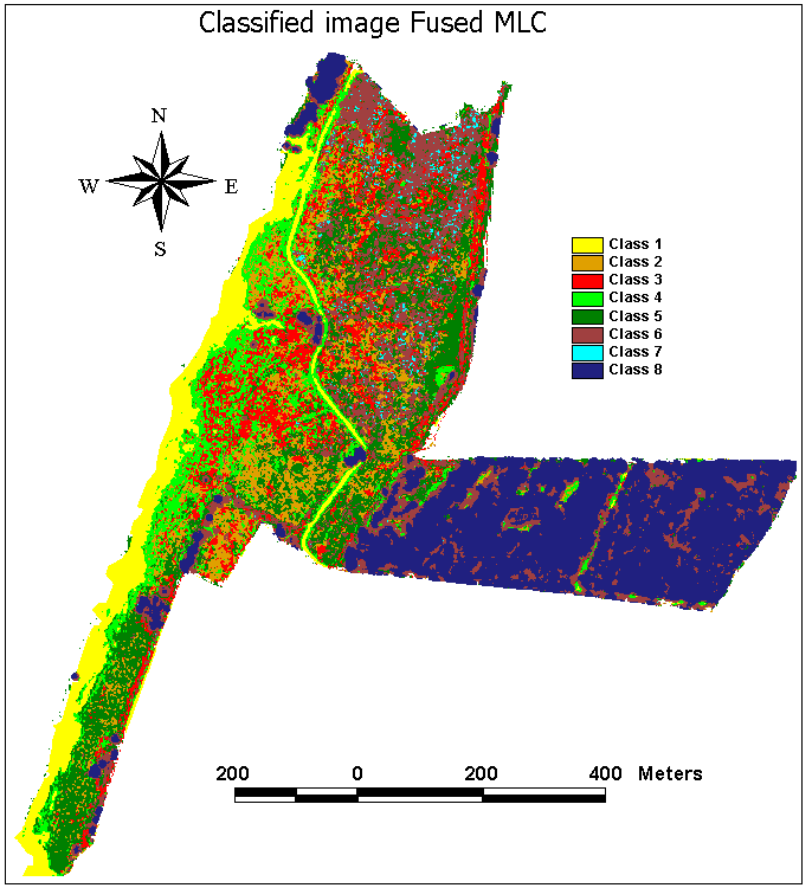

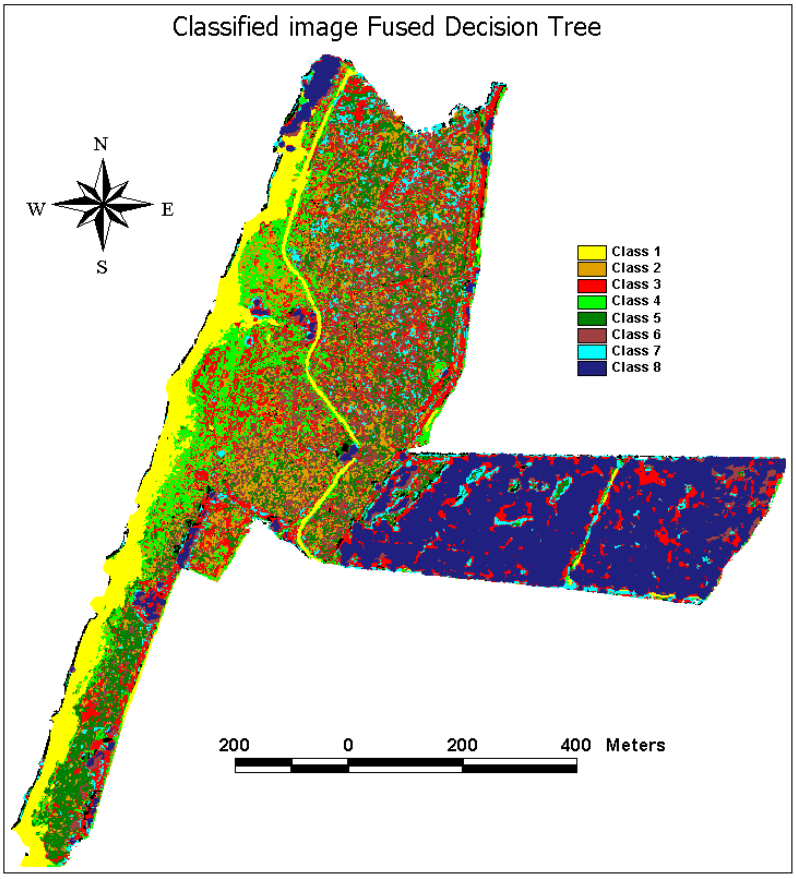

Appendix D

Error Matrix LiDAR 2m circle - - - Overall normalized accuracy: 33.68 %

	Class 1	**Class 2**	**Class 3**	**Class 4**	**Class 5**	**Class 6**	**Class 7**	**Class 8**	norm. user accuracy	producer accuracy
Class 1	**6**	5	7	13	3	4	0	0	31.78%	54.55%
Class 2	2	**11**	9	16	9	4	0	0	13.31%	57.89%
Class 3	2	1	**3**	1	0	4	0	0	7.23%	11.54%
Class 4	0	2	2	**10**	3	4	0	0	22.82%	23.26%
Class 5	1	0	5	3	**1**	3	1	0	8.95%	5.26%
Class 6	0	0	0	0	1	0	1	1	0.00%	0.00%
Class 7	0	0	0	0	2	3	**1**	1	6.78%	33.33%
Class 8	0	0	0	0	0	0	0	**18**	100.00%	90.00%

Appendix E

Error Matrix LiDAR 4m circle - - - Overall normalized accuracy: 43.36 %

	Class 1	**Class 2**	**Class 3**	**Class 4**	**Class 5**	**Class 6**	**Class 7**	**Class 8**	norm. user accuracy	producer accuracy
Class 1	**8**	10	8	21	4	8	0	0	26.64%	72.73%
Class 2	0	**0**	1	0	1	1	0	0	0.00%	0.00%
Class 3	0	2	**4**	1	3	3	0	0	10.63%	15.38%
Class 4	1	6	6	**17**	7	4	0	0	22.89%	39.53%
Class 5	2	1	4	4	**3**	2	0	0	23.88%	15.79%
Class 6	0	0	0	0	1	**3**	0	0	84.76%	13.64%
Class 7	0	0	2	0	0	1	**3**	0	44.94%	100.00%
Class 8	0	0	1	0	0	0	0	**20**	99.07%	100.00%

Appendix F

Error Matrix CASI - - - Overall normalized accuracy: 55.60 %

	Class 1	Class 2	Class 3	Class 4	Class 5	Class 6	Class 7	Class 8	norm. user accuracy	producer accuracy
Class 1	**11**	0	0	1	0	0	1	0	86.90%	100.00%
Class 2	0	**6**	3	9	2	1	0	0	33.63%	31.58%
Class 3	0	2	**11**	9	0	0	0	0	58.58%	42.31%
Class 4	0	2	3	**20**	0	2	0	1	41.04%	46.51%
Class 5	0	2	5	2	**13**	5	0	0	49.40%	68.42%
Class 6	0	5	3	2	2	**12**	1	0	52.76%	54.55%
Class 7	0	2	1	0	1	2	**1**	0	24.90%	33.33%
Class 8	0	0	0	0	1	0	0	**19**	97.33%	95.00%

Appendix G

Error Matrix PCA - - - Overall normalized accuracy: 53.46 %

	class 1	Class 2	Class 3	Class 4	Class 5	Class 6	Class 7	Class 8	norm. user accuracy	producer accuracy
Class 1	**11**	0	0	1	0	0	0	0	91.67%	100.00%
Class 2	0	**3**	2	6	0	3	1	0	21.43%	15.79%
Class 3	0	1	**6**	10	3	1	0	0	28.57%	23.08%
Class 4	0	4	5	**22**	1	0	0	0	68.75%	51.16%
Class 5	0	1	3	1	**8**	1	0	0	57.14%	42.11%
Class 6	0	9	9	3	6	**13**	2	0	30.95%	59.09%
Class 7	0	1	1	0	1	4	**0**	0	0.00%	0.00%
Class 8	0	0	0	0	0	0	0	**20**	100.00%	100.00%

Appendix H

Error Matrix FUSED (Maximum Likelihood Classification) - - - Overall normalized accuracy: 63.52 %

	Class 1	**Class 2**	**Class 3**	**Class 4**	**Class 5**	**Class 6**	**Class 7**	**Class 8**	norm. user accuracy	producer accuracy
Class 1	**11**	0	0	0	0	0	0	0	100.00%	100.00%
Class 2	0	**4**	3	8	2	2	0	0	22.55%	21.05%
Class 3	0	4	**16**	10	2	4	0	0	39.90%	61.54%
Class 4	0	5	4	**23**	3	2	0	0	46.41%	53.49%
Class 5	0	6	3	2	**12**	9	0	0	48.31%	63.16%
Class 6	0	0	0	0	0	**5**	1	0	91.26%	22.73%
Class 7	0	0	0	0	0	0	**2**	0	100.00%	66.67%
Class 8	0	0	0	0	0	0	0	**20**	100.00%	100.00%

Appendix I

Error Matrix FUSED (Decision Tree Classification, CART analysis) - - - Overall normalized accuracy: 53.65 %

	Class 1	**Class 2**	**Class 3**	**Class 4**	**Class 5**	**Class 6**	**Class 7**	**Class 8**	norm. user accuracy	producer accuracy
Class 1	**11**	0	0	0	0	0	0	0	100.00%	100.00%
Class 2	0	**7**	5	7	4	2	0	0	30.85%	36.84%
Class 3	0	1	**7**	7	5	7	2	0	22.62%	26.92%
Class 4	0	6	9	**29**	0	2	0	0	38.74%	67.44%
Class 5	0	2	2	0	**5**	7	0	0	35.56%	26.32%
Class 6	0	3	2	0	4	**3**	0	0	25.27%	13.64%
Class 7	0	0	1	0	1	1	**1**	0	45.07%	33.33%
Class 8	0	0	0	0	0	0	0	**20**	100.00%	100.00%